Article

A Control Scheme to Suppress Circulating Currents in Parallel-Connected Three-Phase Inverters

Marian Liberos * [ID]**, Raúl González-Medina** [ID]**, Iván Patrao** [ID]**, Gabriel Garcerá** [ID] **and Emilio Figueres**

Grupo de Sistemas Electrónicos Industriales, Departamento de Ingeniería Electrónica, Universitat Politècnica de València, Camino de Vera s/n, 46022 Valencia, Spain
*   Correspondence: malimas@upv.es

Abstract: The parallel operation of inverters has many benefits, such as modularity and redundancy. However, the parallel connection of inverters produces circulating currents that may result in malfunctions of the system. In this work, a control technique for the elimination of the low-frequency components of the circulating currents in grid-connected inverters is presented. The proposed control structure contains $n - 1$ zero-sequence control loops, with n being the number of inverters connected in parallel. Simulation and experimental results have been carried out on a prototype composed of two 5 kW inverters connected in parallel. The results have been obtained by considering the following mismatches between both inverters: inductance values of the grid filters, unbalance of the delivered power, and the use of different modulation techniques.

Keywords: control design; PI control; current control; parallel inverter system; space vector modulation (SVM)

1. Introduction

The parallel connection of inverters has been used in various applications, as it has some advantages, such as modularity, redundancy, and easy maintenance [1–3]. However, when there are mismatches in the hardware components, such as the inductance values of the filters or the control parameters of the modules connected in parallel, circulating currents happen to lead to undesirable effects in the system [4–6]. Circulating currents can produce adverse effects, such as the distortion of the AC currents, an unbalance in the power delivered by each inverter, higher conduction losses in the switching devices, and lower efficiency of the whole system.

One of the simplest methods to eliminate circulating currents uses transformers to electrically isolate the parallel connected modules. This method leads to an expensive and bulky system, with control methods not requiring extra hardware being preferred [7–11].

The circulating current is composed of high-frequency harmonics, close to the switching frequency and its multiples, and low-frequency harmonics placed at the fundamental frequency and its multiples. High-frequency circulating currents are usually eliminated using passive elements, as in [12,13]. This work is focused on low-frequency circulating currents.

To reduce circulating currents, in some works, such as [14,15], the n modules connected in parallel have been considered as a single converter that has as many branches as the branches of each module multiplied by n. This control is very complex for high values of n and does not allow for a modular design. Other works, such as [13], proposed a finite time control method. In [16], a double modulation compensation technique was used; in [8], a harmonic elimination PWM modulation (HEPWM) that needs a high switching frequency, leading to high switching losses, was proposed. Other studies proposed the control of the zero-sequence current of the inverters [17,18]. In [17], a common-mode voltage injection PWM method was described, and [18] proposed a multicarrier PWM for parallel three-phase active front-end converters. In both cases, a control action was added to the three control signals of the PWM modulator to reduce the circulating currents. In

those works, the effect that the addition of the proposed control signal had on the stability of the system had not been analyzed. Reference [19] proposed the control of the homopolar component of the phase currents to avoid circulating currents using three-dimensional space vector modulation (3D-SVM).

This paper proposes a control structure based on the fact that the circulating currents among inverters agree with the zero-sequence component of the three-phase currents, so that, by regulating the zero-sequence component to a null setpoint value, circulating currents are eliminated. The complexity of the proposed solution is very low, allowing for a modular design that can be easily extended to a high value of n. Regarding [19], where only differences among inverter inductances were taken into account, the present work considers various causes that produce circulating currents: mismatches in the inductance values of the grid filters among inverters and in each phase of the same inverter, unbalance of the delivered power, and the use of different modulation techniques. In addition, the harmonic contents of the circulating currents have been considered to adjust the resonant controllers in the inverter's current loops, which improves the control action at the frequencies of interest. The control structure proposed in the current work has been validated in an experimental laboratory set-up. The stability of the whole system has been analyzed and supported by both analytical and experimental results.

2. Modeling of n Inverters Connected in Parallel in the Synchronous Reference Frame

Figure 1 shows a general scheme of n inverters connected in parallel. The grid filter of each inverter is an LCL filter with a damping resistance, R_d, connected in series with the filter capacitance, C_f. The inductances of the filter can be implemented by means of three-phase inductors, being L_f and L_{fg}, the inverter-side inductance and grid-side self-inductance, respectively, whereas r_f and r_{fg} are the corresponding parasitic series resistances. M_f and M_{fg} stand for the inverter-side and grid-side mutual inductance values, respectively. The grid impedance at the point of common coupling (PCC) is characterized by its self-inductance, L_g, parasitic series resistance, r_g, and mutual inductance, M_g.
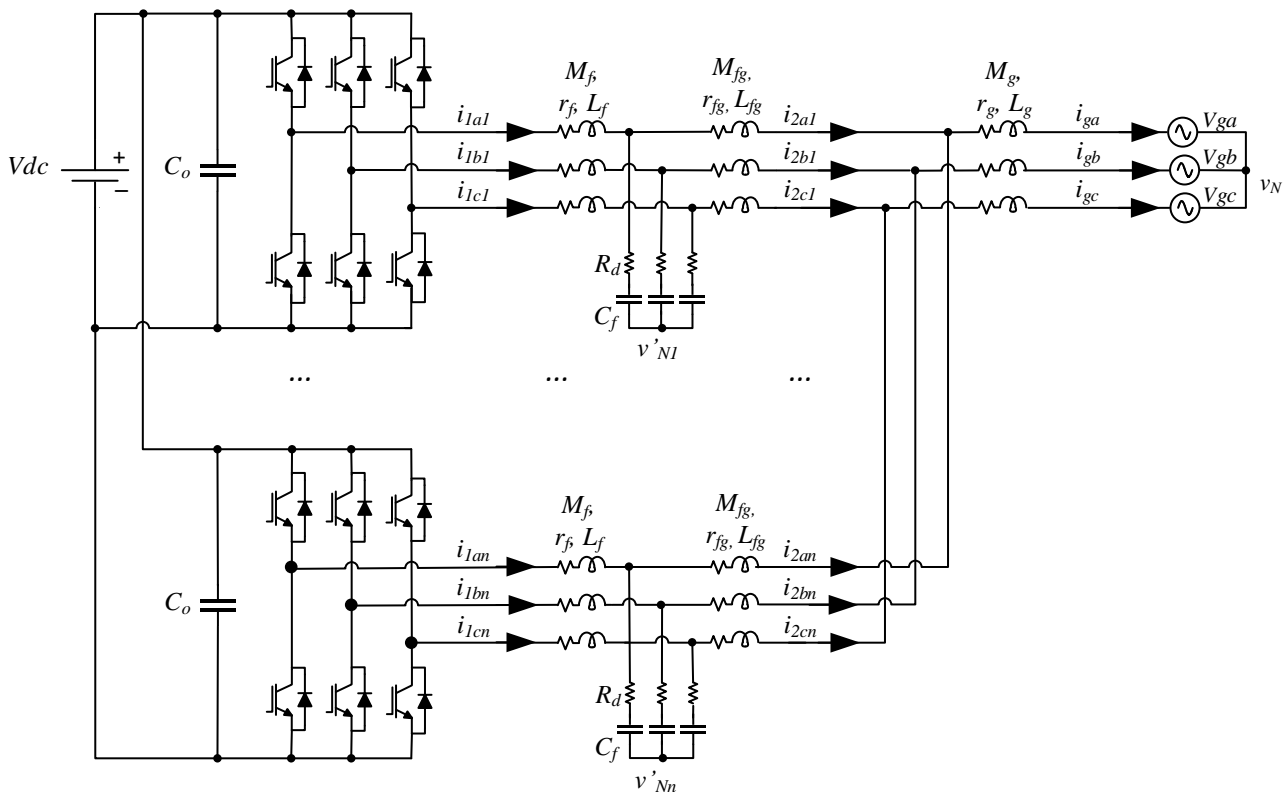

Figure 1. Circuit of the parallel inverters.

The goal of this section is to obtain a MIMO model of the system in a *dqo* synchronous reference frame (SRF), having the grid voltage aligned with the *d*-axis. Then, the active and reactive powers can be regulated with the *d* and *q* components of the AC currents, respectively. It is worth pointing out that the zero-sequence component (channel *o*) of the current is normally omitted in three-phase inverters because this component is naturally zero in the case of three-wire inverters without a neutral conductor. In the proposed control structure, the zero-sequence component will also be regulated.

2.1. Averaged Model Equations

Figure 2 shows the averaged equivalent circuit of Figure 1 represented in the stationary three-phase reference frame. Equations (2)–(6) are obtained from this scheme. In Equations (2)–(6), the value of i ($i = 1, \ldots, n$) identifies each module, with n being the total number of modules. The load factor of each module, c_i, is defined by Equation (1), with $I_{2i\_RMS\_OP}$ being the RMS phase current at the operation point provided by inverter #i and $I_{2i\_RMS\_NOM}$ being its nominal RMS phase current. *Fm* stands for the gain of the SVM modulation and depends on its implementation inside the digital controller in which the control loops are programmed.
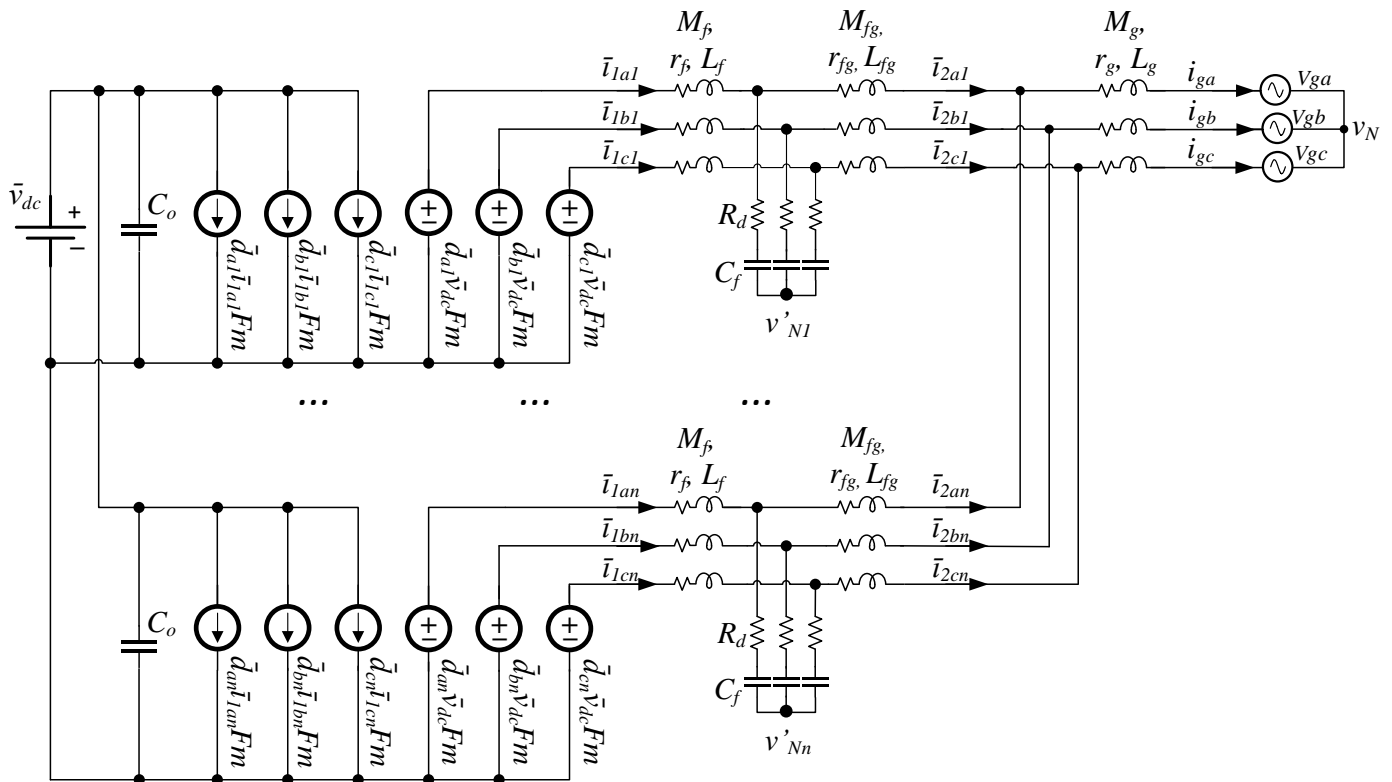

Figure 2. Averaged equivalent circuit of the parallel inverters.

$$c_i = \frac{I_{2i\_RMS_{OP}}}{I_{2i\_RMS_{NOM}}}, \quad i = 1, 2, \ldots n \tag{1}$$

$$\bar{i}_{g\varphi} = \bar{i}_{2\varphi 1} + \bar{i}_{2\varphi 2} + \ldots + \bar{i}_{2\varphi n} = \frac{\sum_{j=1}^{n} c_j}{c_i} \bar{i}_{2\varphi i}, \quad i = 1, 2, \ldots n, \quad \varphi = a, b, c \tag{2}$$

$$\begin{bmatrix} L_f & M_f & M_f \\ M_f & L_f & M_f \\ M_f & M_f & L_f \end{bmatrix} \cdot \frac{d}{dt} \begin{bmatrix} \bar{i}_{1ai} \\ \bar{i}_{1bi} \\ \bar{i}_{1ci} \end{bmatrix} = Fm \cdot \bar{v}_{dc} \begin{bmatrix} \bar{d}_{ai} \\ \bar{d}_{bi} \\ \bar{d}_{ci} \end{bmatrix} - r_f \begin{bmatrix} \bar{i}_{1ai} \\ \bar{i}_{1bi} \\ \bar{i}_{1ci} \end{bmatrix} - \begin{bmatrix} \bar{v}_{cai} \\ \bar{v}_{cbi} \\ \bar{v}_{cci} \end{bmatrix} - R_d \left(\begin{bmatrix} \bar{i}_{1ai} \\ \bar{i}_{1bi} \\ \bar{i}_{1ci} \end{bmatrix} - \begin{bmatrix} \bar{i}_{2ai} \\ \bar{i}_{2bi} \\ \bar{i}_{2ci} \end{bmatrix} \right) - \begin{bmatrix} \bar{v}_{Ni'} \\ \bar{v}_{Ni} \\ \bar{v}_{Ni} \end{bmatrix}, \quad i = 1, 2, \ldots n \tag{3}$$

$$
\begin{bmatrix}
L_{fg}+\frac{\sum_{j=1}^{n}c_j}{c_i}L_g & M_{fg}+\frac{\sum_{j=1}^{n}c_j}{c_i}M_g & M_{fg}+\frac{\sum_{j=1}^{n}c_j}{c_i}M_g \\
M_{fg}+\frac{\sum_{j=1}^{n}c_j}{c_i}M_g & L_{fg}+\frac{\sum_{j=1}^{n}c_j}{c_i}L_g & M_{fg}+\frac{\sum_{j=1}^{n}c_j}{c_i}M_g \\
M_{fg}+\frac{\sum_{j=1}^{n}c_j}{c_i}M_g & M_{fg}+\frac{\sum_{j=1}^{n}c_j}{c_i}M_g & L_{fg}+\frac{\sum_{j=1}^{n}c_j}{c_i}L_g
\end{bmatrix}\cdot\frac{d}{dt}
\begin{bmatrix}\bar{i}_{2ai}\\ \bar{i}_{2bi}\\ \bar{i}_{2ci}\end{bmatrix}
$$
$$
=\begin{bmatrix}\bar{v}_{Ni}\\ \bar{v}_{Ni}\\ \bar{v}_{Ni}\end{bmatrix}
-\left(r_{fg}+\frac{\sum_{j=1}^{n}c_j}{c_i}r_g\right)\begin{bmatrix}\bar{i}_{2ai}\\ \bar{i}_{2bi}\\ \bar{i}_{2ci}\end{bmatrix}
+\begin{bmatrix}\bar{v}_{cai}\\ \bar{v}_{cbi}\\ \bar{v}_{cci}\end{bmatrix}
+R_d\left(\begin{bmatrix}\bar{i}_{1ai}\\ \bar{i}_{1bi}\\ \bar{i}_{1ci}\end{bmatrix}-\begin{bmatrix}\bar{i}_{2ai}\\ \bar{i}_{2bi}\\ \bar{i}_{2ci}\end{bmatrix}\right)
-\begin{bmatrix}\bar{v}_{ga}\\ \bar{v}_{gb}\\ \bar{v}_{gc}\end{bmatrix}
-\begin{bmatrix}\bar{v}_{Ni}\\ \bar{v}_{Ni}\\ \bar{v}_{Ni}\end{bmatrix}, \quad i=1,2,\ldots n
\tag{4}
$$

$$
\frac{d}{dt}\begin{bmatrix}\bar{v}_{cai}\\ \bar{v}_{cbi}\\ \bar{v}_{cci}\end{bmatrix}=\frac{1}{C_f}\left(\begin{bmatrix}\bar{i}_{1ai}\\ \bar{i}_{1bi}\\ \bar{i}_{1ci}\end{bmatrix}-\begin{bmatrix}\bar{i}_{2ai}\\ \bar{i}_{2bi}\\ \bar{i}_{2ci}\end{bmatrix}\right),\quad i=1,2,\ldots n
\tag{5}
$$

$$
\frac{d}{dt}\bar{v}_{dc}=\frac{1}{nC_o}\left(\bar{i}_{dc}-Fm\begin{bmatrix}\bar{d}_{a1}\\ \bar{d}_{b1}\\ \bar{d}_{c1}\end{bmatrix}^T\begin{bmatrix}\bar{i}_{1a1}\\ \bar{i}_{1b1}\\ \bar{i}_{1c1}\end{bmatrix}-Fm\begin{bmatrix}\bar{d}_{a2}\\ \bar{d}_{b2}\\ \bar{d}_{c2}\end{bmatrix}^T\begin{bmatrix}\bar{i}_{1a2}\\ \bar{i}_{1b2}\\ \bar{i}_{1c2}\end{bmatrix}-\cdots-Fm\begin{bmatrix}\bar{d}_{an}\\ \bar{d}_{bn}\\ \bar{d}_{cn}\end{bmatrix}^T\begin{bmatrix}\bar{i}_{1an}\\ \bar{i}_{1bn}\\ \bar{i}_{1cn}\end{bmatrix}\right)
\tag{6}
$$

It is worth pointing out that the circulating currents comply with Equation (7), so it is only necessary to regulate the $n-1$ zero-sequence currents (i_{o1} to i_{on}) to zero, being null to the zero-sequence duty cycle of the *n-th* converter. Taking into account that the filter capacitors are not connected to the midpoint of the dc-link, the circulating currents neither flow through them nor to the grid, as it was shown in [12]. In view of this, and following the procedure described in Appendix A, the equations in the SRF have been obtained, Equations (8)–(12).

$$
\bar{i}_{on}=-\left(\bar{i}_{o1}+\bar{i}_{o2}+\ldots\bar{i}_{o(n-1)}\right)
\tag{7}
$$

$$
\frac{d}{dt}\begin{bmatrix}\bar{i}_{1di}\\ \bar{i}_{1qi}\end{bmatrix}=-\begin{bmatrix}0 & -\omega\\ \omega & 0\end{bmatrix}\begin{bmatrix}\bar{i}_{1di}\\ \bar{i}_{1qi}\end{bmatrix}+\frac{Fm\bar{v}_{dc}}{L_f-M_f}\begin{bmatrix}\bar{d}_{di}\\ \bar{d}_{qi}\end{bmatrix}-\frac{1}{L_f-M_f}\begin{bmatrix}\bar{v}_{cdi}\\ \bar{v}_{cqi}\\ \bar{v}_{coi}\end{bmatrix}-\frac{R_d+r_f}{L_f-M_f}\begin{bmatrix}\bar{i}_{1di}\\ \bar{i}_{1qi}\end{bmatrix}+\frac{R_d}{L_f-M_f}\begin{bmatrix}\bar{i}_{2di}\\ \bar{i}_{2qi}\end{bmatrix},\ i=1,2,\ldots n
\tag{8}
$$

$$
\begin{aligned}
\frac{d}{dt}\begin{bmatrix}\bar{i}_{2di}\\ \bar{i}_{2qi}\end{bmatrix}=&-\begin{bmatrix}0 & -\omega\\ \omega & 0\end{bmatrix}\begin{bmatrix}\bar{i}_{2di}\\ \bar{i}_{2qi}\end{bmatrix}+\frac{1}{L_{fg}-M_{fg}+\frac{\sum_{j=1}^{n}c_j}{c_i}\left(L_g-M_g\right)}\begin{bmatrix}\bar{v}_{cdi}\\ \bar{v}_{cqi}\end{bmatrix}+\frac{R_d}{L_{fg}-M_{fg}+\frac{\sum_{j=1}^{n}c_j}{c_i}\left(L_g-M_g\right)}\begin{bmatrix}\bar{i}_{1di}\\ \bar{i}_{1qi}\end{bmatrix}\\
&-\frac{R_d+r_{fg}+\frac{\sum_{j=1}^{n}c_j}{c_i}r_c}{L_{fg}-M_{fg}+\frac{\sum_{j=1}^{n}c_j}{c_i}\left(L_g-M_g\right)}\begin{bmatrix}\bar{i}_{2di}\\ \bar{i}_{2qi}\end{bmatrix}-\frac{1}{L_{fg}-M_{fg}+\frac{\sum_{j=1}^{n}c_j}{c_i}\left(L_g-M_g\right)}\begin{bmatrix}\bar{v}_{gd}\\ \bar{v}_{gq}\end{bmatrix},\quad i=1,2,\ldots n
\end{aligned}
\tag{9}
$$

$$
\begin{aligned}
\frac{d}{dt}\begin{bmatrix}\bar{i}_{o1}\\ \bar{i}_{o2}\\ \cdots\\ \bar{i}_{o(n-1)}\end{bmatrix}=&-\begin{bmatrix}
\frac{r_f+r_{fg}}{L_f+L_{fg}+2M_f+2M_{fg}} & 0 & \cdots & 0\\
0 & \frac{r_f+r_{fg}}{L_f+L_{fg}+2M_f+2M_{fg}} & \cdots & 0\\
\vdots & \vdots & \ddots & \vdots\\
0 & 0 & \cdots & \frac{r_f+r_{fg}}{L_f+L_{fg}+2M_f+2M_{fg}}
\end{bmatrix}\begin{bmatrix}\bar{i}_{o1}\\ \bar{i}_{o2}\\ \cdots\\ \bar{i}_{o(n-1)}\end{bmatrix}\\
&+\begin{bmatrix}
\frac{(n-1)Fm\bar{v}_{dc}}{n\left(L_f+L_{fg}+2M_f+2M_{fg}\right)} & \frac{-Fm\bar{v}_{dc}}{n\left(L_f+L_{fg}+2M_f+2M_{fg}\right)} & \cdots & \frac{-Fm\bar{v}_{dc}}{n\left(L_f+L_{fg}+2M_f+2M_{fg}\right)}\\
\frac{-Fm\bar{v}_{dc}}{n\left(L_f+L_{fg}+2M_f+2M_{fg}\right)} & \frac{(n-1)Fm\bar{v}_{dc}}{n\left(L_f+L_{fg}+2M_f+2M_{fg}\right)} & \cdots & \frac{-Fm\bar{v}_{dc}}{n\left(L_f+L_{fg}+2M_f+2M_{fg}\right)}\\
\vdots & \vdots & \ddots & \vdots\\
\frac{-Fm\bar{v}_{dc}}{n\left(L_f+L_{fg}+2M_f+2M_{fg}\right)} & \frac{-Fm\bar{v}_{dc}}{n\left(L_f+L_{fg}+2M_f+2M_{fg}\right)} & \cdots & \frac{(n-1)Fm\bar{v}_{dc}}{n\left(L_f+L_{fg}+2M_f+2M_{fg}\right)}
\end{bmatrix}
\end{aligned}
\tag{10}
$$

$$
\frac{d}{dt}\begin{bmatrix}\bar{v}_{cdi}\\ \bar{v}_{cqi}\end{bmatrix}=-\begin{bmatrix}0 & -\omega\\ \omega & 0\end{bmatrix}\begin{bmatrix}\bar{v}_{cdi}\\ \bar{v}_{cqi}\end{bmatrix}+\frac{1}{C_f}\left(\begin{bmatrix}\bar{i}_{1di}\\ \bar{i}_{1qi}\end{bmatrix}-\begin{bmatrix}\bar{i}_{2di}\\ \bar{i}_{2qi}\end{bmatrix}\right),\quad i=1,2,\ldots n
\tag{11}
$$

$$\frac{d}{dt}\overline{v}_{dc} = \frac{1}{nC_o}\left(\overline{i}_{pv} - Fm\begin{bmatrix}\overline{d}_{d1}\\\overline{d}_{q1}\\\overline{d}_{o1}\end{bmatrix}^T\begin{bmatrix}\overline{i}_{1d1}\\\overline{i}_{1q1}\\\overline{i}_{o1}\end{bmatrix} - Fm\begin{bmatrix}\overline{d}_{d2}\\\overline{d}_{q2}\\\overline{d}_{o2}\end{bmatrix}^T\begin{bmatrix}\overline{i}_{1d2}\\\overline{i}_{1q2}\\\overline{i}_{o2}\end{bmatrix} - \cdots - \cdots - Fm\begin{bmatrix}\overline{d}_{dn-1}\\\overline{d}_{qn-1}\\\overline{d}_{on-1}\end{bmatrix}^T\begin{bmatrix}\overline{i}_{1d(n-1)}\\\overline{i}_{1q(n-1)}\\\overline{i}_{o(n-1)}\end{bmatrix} \\ - Fm\begin{bmatrix}\overline{d}_{dn}\\\overline{d}_{qn}\end{bmatrix}^T\begin{bmatrix}\overline{i}_{1dn}\\\overline{i}_{1qn}\end{bmatrix}\right) \tag{12}$$

2.2. Derivation of the Small Signal MIMO Model

The small signal model of the parallel inverters has been obtained in this section. It has been obtained by applying Equation (13) to SRF Equations (8)–(12). In Equation (13), $\overline{x}$ stands for each of the variables of the averaged model, expressed as the sum of the value at the operation point, X, and the small signal value, $\hat{x}$.

$$\overline{x} = X + \hat{x} \tag{13}$$

The equations of the small signal model in the SRF frame are expressed in Equations (14)–(21). Because of the model complexity, some auxiliary matrices (A9)–(A25) have been defined to simplify A, B, C, and D. The input vector U defines the control variables (the duty cycle of each branch of the inverter) and the disturbances (the grid voltage). The constant K_{vo} is expressed by Equation (A19), considering that at the DC side, there is a constant power load (CPL) or a photovoltaic field that can be modelled as a current source.

$$\frac{\mathrm{d}}{\mathrm{d}t}X = A{\cdot}X + B{\cdot}U \tag{14}$$

$$Y = C{\cdot}X + D{\cdot}U \tag{15}$$

$$X = Y = \begin{bmatrix} \hat{i}_{1d1} & \hat{i}_{1q1} & \hat{i}_{2d1} & \hat{i}_{2q1} & \hat{i}_{o1} & \hat{v}_{cd1} & \hat{v}_{cq1} & \cdots & \hat{i}_{1d(n-1)} & \hat{i}_{1q(n-1)} & \hat{i}_{2d(n-1)} & \hat{i}_{2q(n-1)} & \hat{i}_{o(n-1)} & \hat{v}_{cd(n-1)} & \hat{v}_{cq(n-1)} \\ & & & \hat{i}_{1dn} & \hat{i}_{1qn} & \hat{i}_{2dn} & \hat{i}_{2qn} & \hat{v}_{cdn} & \hat{v}_{cqn} & \hat{v}_{dc} \end{bmatrix}^T \tag{16}$$

$$U = \begin{bmatrix} \hat{d}_{d1} \ \hat{d}_{q1} \ \hat{d}_{o1} \ \cdots \ \hat{d}_{d(n-1)} \ \hat{d}_{q(n-1)} \ \hat{d}_{o(n-1)} \ \hat{d}_{dn} \ \hat{d}_{qn} \ \hat{v}_{gd} \ \hat{v}_{gq} \ \hat{v}_{go} \end{bmatrix}^T \tag{17}$$

$$A = \begin{bmatrix}
A_{\hat{i}12dq\_i12dq} & 0 & A_{\hat{i}12dq\_vcdq} & \cdots & 0 & 0 & 0 & \cdots & 0 & 0 & A_{\hat{i}12dq\_vdc} \\
0 & A_{\hat{i}o\_io} & 0 & \cdots & 0 & 0 & 0 & \cdots & 0 & 0 & A_{\hat{i}o\_vdc} \\
A_{\hat{v}cdq\_i12dq} & 0 & A_{\hat{v}cdq\_vcdq} & \cdots & 0 & 0 & 0 & \cdots & 0 & 0 & 0 \\
\vdots & \vdots & \vdots & \ddots & \vdots & \vdots & \vdots & \ddots & \vdots & \vdots & \vdots \\
0 & 0 & 0 & \cdots & A_{\hat{i}12dq\_i12dq} & 0 & A_{\hat{i}12dq\_vcdq} & \cdots & 0 & 0 & A_{\hat{i}12dq\_vdc} \\
0 & 0 & 0 & \cdots & 0 & A_{\hat{i}o\_io} & 0 & \cdots & 0 & 0 & A_{\hat{i}o\_vdc} \\
0 & 0 & 0 & \cdots & A_{\hat{v}cdq\_i12dq} & 0 & A_{\hat{v}cdq\_vcdq} & \cdots & 0 & 0 & 0 \\
\vdots & \vdots & \vdots & \ddots & \vdots & \vdots & \vdots & \ddots & \vdots & \vdots & \vdots \\
0 & 0 & 0 & \cdots & 0 & 0 & 0 & \cdots & A_{\hat{i}12dq\_i12dq} & A_{\hat{i}12dq\_vcdq} & A_{\hat{i}12dq\_vdc} \\
0 & 0 & 0 & \cdots & 0 & 0 & 0 & \cdots & A_{\hat{v}cdq\_i12dq} & A_{\hat{v}cdq\_vcdq} & 0 \\
A_{\hat{v}dc\_i12dq} & A_{\hat{v}dc\_io} & 0 & \cdots & A_{\hat{v}dc\_i12dq} & A_{\hat{v}dc\_io} & 0 & \cdots & A_{\hat{v}dc\_i12dq} & 0 & A_{\hat{v}dc\_vdc}
\end{bmatrix} \tag{18}$$

$$B = \begin{bmatrix} B_{\hat{i}12dq\_ddq} & 0 & \cdots & 0 & 0 & 0 & B_{\hat{i}12dq\_vgdqo} \\ 0 & B_{\hat{io}\_doi} & \cdots & 0 & B_{\hat{io}\_do} & 0 & 0 \\ 0 & 0 & \cdots & 0 & 0 & 0 & 0 \\ \vdots & \vdots & \ddots & \vdots & \vdots & \vdots & \vdots \\ 0 & 0 & \cdots & B_{\hat{i}12dq\_ddq} & 0 & 0 & B_{\hat{i}12dq\_vgdqo} \\ 0 & B_{\hat{io}\_do} & \cdots & 0 & B_{\hat{io}\_doi} & 0 & 0 \\ 0 & 0 & \cdots & 0 & 0 & 0 & 0 \\ \vdots & \vdots & \ddots & \vdots & \vdots & \vdots & \vdots \\ 0 & 0 & \cdots & 0 & 0 & B_{\hat{i}12dq\_ddq} & B_{\hat{i}12dq\_vgdqo} \\ 0 & 0 & \cdots & 0 & 0 & 0 & 0 \\ B_{\hat{vdc}\_ddq} & B_{\hat{vdc}\_do} & \cdots & B_{\hat{vdc}\_ddq} & B_{\hat{vdc}\_do} & B_{\hat{vdc}\_ddq} & 0 \end{bmatrix} \tag{19}$$

$$C = I \tag{20}$$

$$D = 0 \tag{21}$$

The expressions of the variables at the operation point are summarized in Table 1. In order to simplify their calculation, the inductor resistances have been neglected, as well as the filter capacitors, so that the currents at the grid side (I_{1dqi}) and at the converter side (I_{2dqi}) agree ($I_{dqi} \approx I_{1dqi} \approx I_{2dqi}$). In addition, the expressions of the operation point have been obtained by considering the control objectives. Since zero reactive power and zero circulating currents are aimed at, both the reactive and zero-sequence components of the currents are chosen to be null. The value of the load factor for each inverter, c_i, can vary between 0 and 1.

Table 1. Expression of the variables in the operation point.

Variable	Expression
V_{gd}	V_{gRMS} (*phase–phase*)
V_{gq}	0
V_{go}	0
I_{di}	$\frac{I_{dc\_nom}}{n \cdot Fm \cdot D_{di}} c_i,\ i = 1, 2, \ldots n$
I_{qi}	0
I_{oi}	0
D_{di}	$\frac{V_{gd}}{Fm \cdot V_{dc}}$
D_{qi}	$\dfrac{\omega I_{di}\left(L_f + L_{fg} - M_f - M_{fg} + \frac{\sum_{j=1}^{n} c_j}{c_i}\left(L_g - M_g\right)\right)}{Fm \cdot Vdc},\ i = 1, 2, \ldots n$
D_{oi}	0

3. Control Architecture

Figure 3 shows the scheme of the proposed control scheme. It is composed of n current control loops for d- and q-channels (in both cases, one per inverter) and $n - 1$ current control loops for regulating the o-channel.

By aligning the d-axis of the reference frame with the direct-sequence fundamental space vector of the grid voltage, the active power may be controlled by regulating the d component of the current, whereas the reactive power can be controlled by acting on the q-axis component. In this case, the reference for the q-axis current is zero, $i_q^* = 0$, in order to obtain a unity power factor. The references in the d- and o- axis are defined by i$_d$* and i$_o$*, respectively.

In three-phase inverters, the zero-sequence component of the phase currents represents the circulating currents among the inverters. The zero-sequence component is defined as one-third of the sum of the phase currents provided by an inverter, $i_o = (i_a + i_b + i_c)/3$. If only one inverter is connected, $i_{o1} = 0$, as the sum of the three-phase currents is zero by application of Kirchhoff's first law ($i_{a1} + i_{b1} + i_{c1} = 0$). If two inverters are connected in parallel, $n = 2$, $i_{o1} = -i_{o2}$, and the circulating currents can be controlled with only one

zero-sequence current control. When there are n inverters connected in parallel, they need $n - 1$ zero-sequence current control regulators. As has been previously pointed out, there is no need to control the zero-sequence component of a three-wire, three-phase inverter when it is operating as a single inverter. However, that is not true in the case of the parallel connection of inverters due to the existence of circulating currents, which are directly related to the zero-sequence component. Therefore, in the proposed solution, the zero-sequence components are controlled with a reference signal $i_o* = 0$ to suppress the circulating currents among inverters.
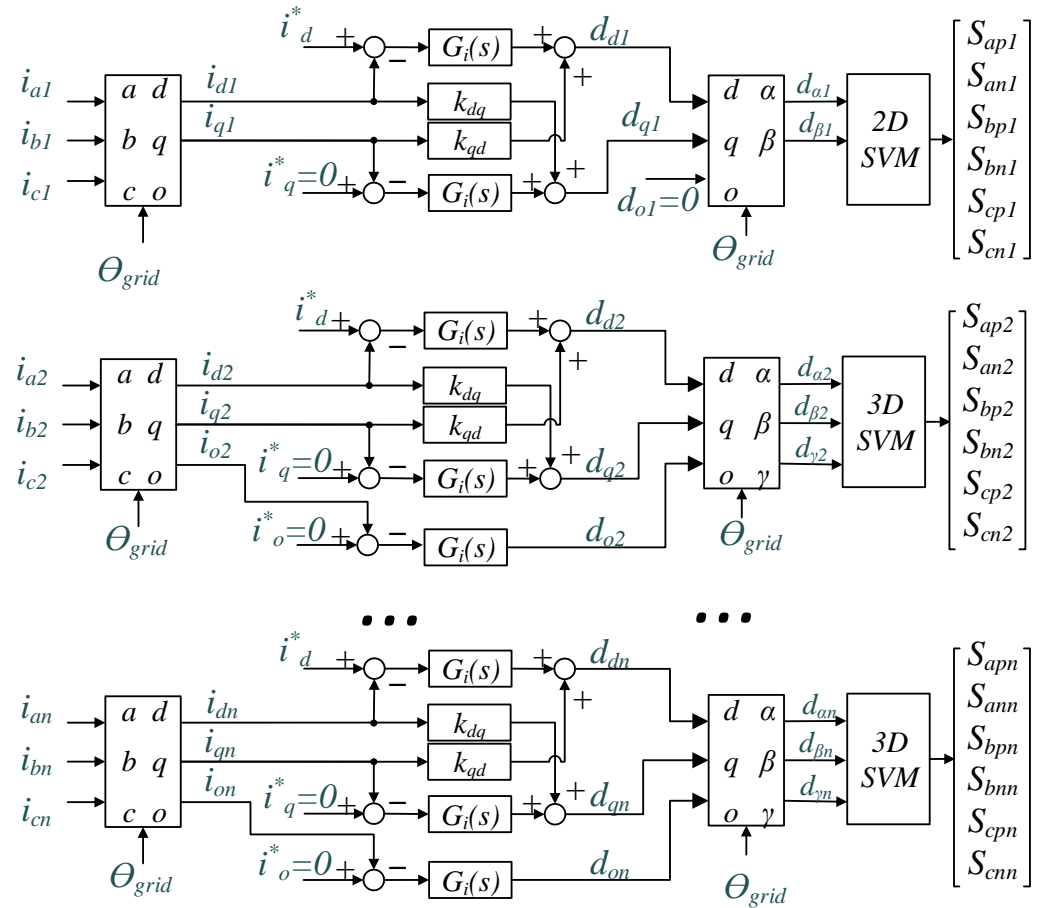

Figure 3. Scheme of the proposed control stage.

Although the zero-sequence components of the currents can be controlled by means of a sinusoidal PWM modulation, the use of SVM modulation has been preferred. The reason is that SVM modulations are digital, so they allow for a much more flexible trip sequence of the transistors than analog PWM modulations. Generally, in three-phase, three-wire systems, 2D-SVM, or simply SVM, is used. However, to control the zero-sequence component of the currents, 3D-SVM is needed, since the three components $\alpha\beta o$ of the phase voltage can be controlled in the whole operation range of the inverter.

When inverters are represented in the synchronous reference frame, coupling terms between the d- and q-axis of the phase currents appear. Equations (24) and (25) express the proposed decoupling terms between both axes, which have been calculated by omitting the effect of the filter capacitors. Under this assumption, the currents at the inverter side (I_{1dqoi}) and at the grid side (I_{2dqoi}) agree ($I_{dqoi} \approx I_{1dqoi} \approx I_{2dqoi}$). Assuming no disturbances, both at the DC-link voltage and at the grid voltage, $\hat{v}_{dc}(s) = \hat{v}_{gd}(s) = 0$, and Equation (22) is obtained. Since ε_{idi} is the current error signal in the d-axis and G_i is the current regulator transfer function, the control action in channel d- can be expressed according to Equation (23). The decoupling term K_{qd} is obtained from Equations (22) and (23). The ex-

pression of K_{dq} is calculated similarly. The decoupling terms are valid from DC to medium frequencies, where the effect of the filter capacitance in the coupling can be neglected.

Note that the decoupling terms depend on the number of inverters on stream, n. If the grid inductances are negligible, the parameters L_g and M_g could be considered null, so that the decoupling terms would be constantly independent of n. However, for the cases where the value of L_g and M_g could not be considered zero, it is easy to automatically readjust the value of the decoupling terms by stocking the needed value as a function of n.

$$
\hat{d}_{di}(s) \cdot Fm \cdot V_{dc} + \omega \left(L_f - M_f + L_{fg} - M_{fg} + \frac{\sum_{j=1}^{n} c_j}{c_i} \left(L_g - M_g \right) \right) \cdot \hat{i}_{qi}(s)
$$

$$
= \left(L_f - M_f + L_{fg} - M_{fg} + \frac{\sum_{j=1}^{n} c_j}{c_i} \left(L_g - M_g \right) \right) s \cdot \hat{i}_{di}(s), \quad i = 1, 2, \dots n \tag{22}
$$

$$
\hat{d}_{di}(s) = G_i(s) \hat{\varepsilon}_{idi}(s) + K_{qdi} \cdot \hat{i}_{qi}(s), \quad i = 1, 2, \dots n \tag{23}
$$

$$
k_{qdi} = - \frac{\omega \left(L_f - M_f + L_{fg} - M_{fg} + \frac{\sum_{j=1}^{n} c_j}{c_i} \left(L_g - M_g \right) \right)}{Fm \cdot V_{dc}}, \quad i = 1, 2, \dots n \tag{24}
$$

$$
k_{dqi} = \frac{\omega \left(L_f - M_f + L_{fg} - M_{fg} + \frac{\sum_{j=1}^{n} c_j}{c_i} \left(L_g - M_g \right) \right)}{Fm \cdot V_{dc}}, \quad i = 1, 2, \dots n \tag{25}
$$

Equations (26)–(28) express the current control open loop gains in channels d, q, and o, respectively. In those equations, R_s is the gain of the current sensor, $G_i(s)$ is the current regulator transfer function, $D(s)$ represents the transfer function of a delay equal to a switching period, which has been calculated from a second-order Padé approximation, and $FPB(s)$ is the transfer function of a low-pass antialiasing filter implemented in the current sensors. The transfer functions of the current as a function of the duty cycle has been obtained from the state space model of the system using MATLAB™ (R2018b). The current sensors have been located at the inverter side of the LCL filter. Placing the sensors at the inverter side, instead of sensing the currents at the grid side, provides higher robustness to the control system [20].

$$
T_{idi}(s) = R_s \cdot G_i(s) \cdot D(s) \cdot FPB(s) \cdot \frac{\hat{i}_{i1di}(s)}{\hat{d}_{di}(s)}, \quad i = 1, 2, \dots n \tag{26}
$$

$$
T_{iqi}(s) = R_s \cdot G_i(s) \cdot D(s) \cdot FPB(s) \cdot \frac{\hat{i}_{i1qi}(s)}{\hat{d}_{qi}(s)}, \quad i = 1, 2, \dots n \tag{27}
$$

$$
T_{ioi}(s) = R_s \cdot G_i(s) \cdot D(s) \cdot FPB(s) \cdot \frac{\hat{i}_{i1oi}(s)}{\hat{d}_{oi}(s)}, \quad i = 1, 2, \dots n \tag{28}
$$

4. Three-Dimension Space Vector Modulator

If the fundamental components of the phase currents are balanced in a three-phase, two-level inverter, the fundamental component of the voltage between the midpoint of the dc-link and the neutral point of the grid is zero. Thus, in that case, it can be considered a virtual connection at the fundamental frequency of the line voltage between the neutral point of the grid and the midpoint of the dc-link [21]. This is an important difference, with respect to three-phase inverters with a four-wire output (three phases + neutral), where the neutral is physically connected. Three-dimensional SVM modulators have been developed for four-wire connected inverters, and, to the best of the authors' knowledge, the first time 3D-SVM was applied to three-phase inverters without neutral was in this work.

Table 2 shows the phase-to-neutral voltage in *abc* coordinates using the DC voltage *vdc* as a reference of the eight possible switching vectors with the considerations described above. It also shows the same voltage in the $\alpha\beta0$ coordinates (Clarke). Figure 4a shows the

twelve tetrahedra, which are defined by two consecutive nonzero switching vectors (in Clarke coordinates) and neutral vectors v_0 and v_7, alternately. The composition of the above tetrahedra defines the whole operation range of the inverter represented in Figure 4b.

Table 2. 3D-SVM switching vectors.

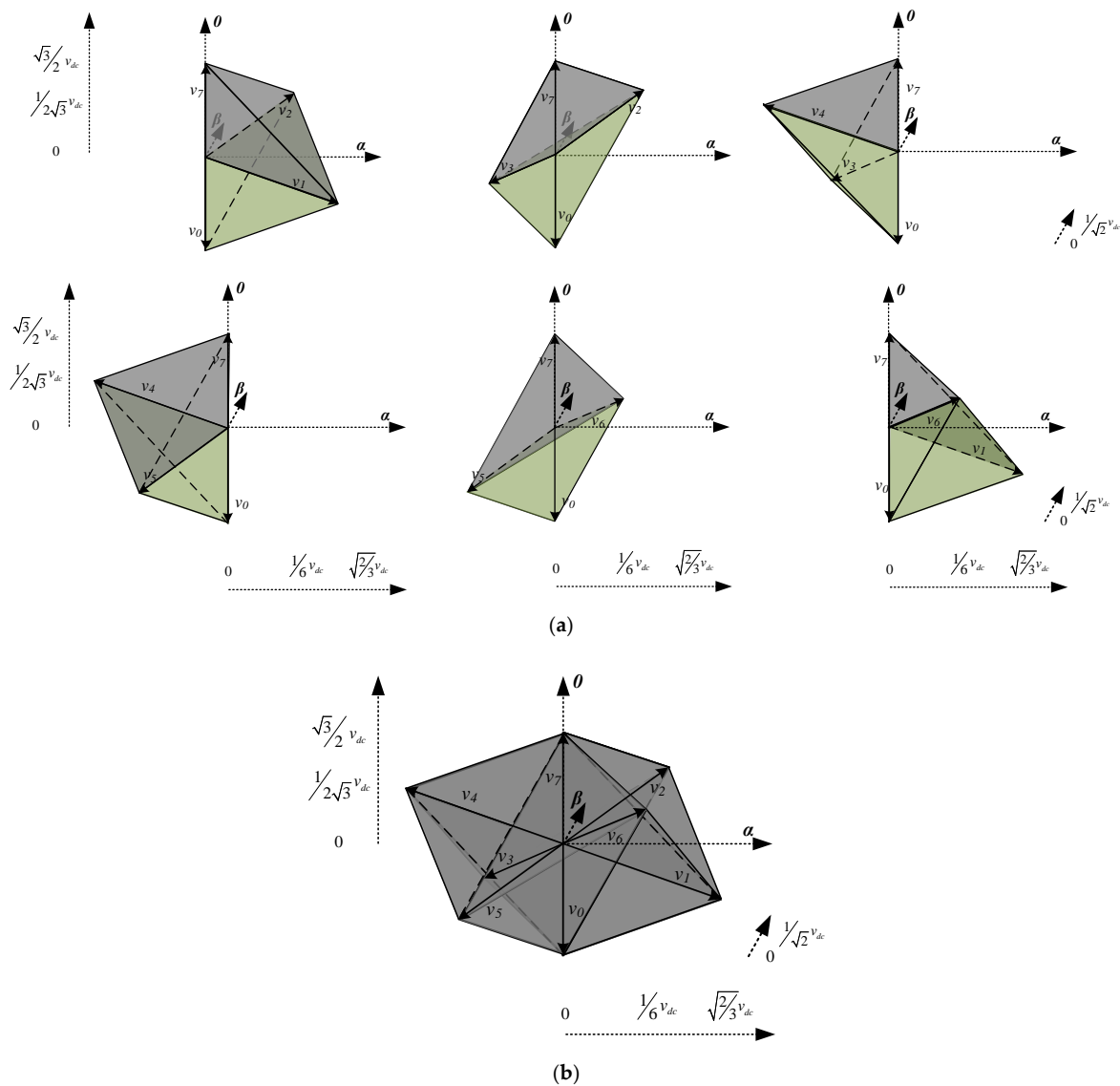| v_φ	$v_{0\text{-}000}$	$v_{1\text{-}100}$	$v_{2\text{-}110}$	$v_{3\text{-}010}$	$v_{4\text{-}011}$	$v_{5\text{-}001}$	$v_{6\text{-}101}$
v_A	$-\frac{1}{2}v_{dc}$	$\frac{1}{2}v_{dc}$	$\frac{1}{2}v_{dc}$	$-\frac{1}{2}v_{dc}$	$-\frac{1}{2}v_{dc}$	$-\frac{1}{2}v_{dc}$	$\frac{1}{2}v_{dc}$
v_B	$-\frac{1}{2}v_{dc}$	$-\frac{1}{2}v_{dc}$	$\frac{1}{2}v_{dc}$	$\frac{1}{2}v_{dc}$	$\frac{1}{2}v_{dc}$	$-\frac{1}{2}v_{dc}$	$-\frac{1}{2}v_{dc}$
v_C	$-\frac{1}{2}v_{dc}$	$-\frac{1}{2}v_{dc}$	$-\frac{1}{2}v_{dc}$	$-\frac{1}{2}v_{dc}$	$\frac{1}{2}v_{dc}$	$\frac{1}{2}v_{dc}$	$\frac{1}{2}v_{dc}$
v_α	0	$\sqrt{\frac{2}{3}}v_{dc}$	$\frac{1}{\sqrt{6}}v_{dc}$	$-\frac{1}{\sqrt{6}}v_{dc}$	$-\sqrt{\frac{2}{3}}v_{dc}$	$-\frac{1}{\sqrt{6}}v_{dc}$	$\frac{1}{\sqrt{6}}v_{dc}$
v_β	0	0	$\frac{1}{\sqrt{2}}v_{dc}$	$\frac{1}{\sqrt{2}}v_{dc}$	0	$-\frac{1}{\sqrt{2}}v_{dc}$	$-\frac{1}{\sqrt{2}}v_{dc}$
v_O	$\frac{-\sqrt{3}}{2}v_{dc}$	$\frac{-1}{2\sqrt{3}}v_{dc}$	$\frac{1}{2\sqrt{3}}v_{dc}$	$\frac{-1}{2\sqrt{3}}v_{dc}$	$\frac{1}{2\sqrt{3}}v_{dc}$	$\frac{-1}{2\sqrt{3}}v_{dc}$	$\frac{1}{2\sqrt{3}}v_{dc}$

(a)

(b)

Figure 4. Spatial representation of the 3D-SVM switching vectors. (**a**) Two tetrahedra composed of two consecutive nonzero switching vectors and neutral vectors v_0 and v_7 (**b**) Spatial representation of the twelve tetrahedra.

Vector modulation consists of constructing the reference voltage vector v^* at the inverter output by alternately applying its adjacent switching vectors. First, the tetrahedron containing the reference vector must be obtained. Once the tetrahedron containing the reference vector is defined, the switching vectors adjacent to v^* are known. From the projections of the reference vector on the switching vectors that delimit the tetrahedron, the time that each switching vector must be applied was calculated in [21–23]. In this work, a symmetric distribution of the switching vectors has been implemented. Table 3 represents the sequence of the switching vectors applied in each prism.

Table 3. Sequence of switching vectors in each prism.

Prism	Sequence of Switching Vectors
I	v_7-v_2-v_1-v_0-v_1-v_2-v_7
II	v_7-v_2-v_3-v_0-v_3-v_2-v_7
III	v_7-v_4-v_3-v_0-v_3-v_4-v_7
IV	v_7-v_4-v_5-v_0-v_5-v_4-v_7
V	v_7-v_6-v_5-v_0-v_5-v_6-v_7
VI	v_7-v_6-v_1-v_0-v_1-v_6-v_7

5. Experimental Set-Up

A 10 kW prototype composed of two three-phase 5 kW inverters has been built and experimentally tested. Figure 5 shows the single-line scheme of the converters, whereas Table 4 summarizes the parameters of the system. As can be seen from Figure 5, the grid filter was an LCL grid filter composed of C_f capacitors with R_d damping resistors, three single-phase inductances at the inverter side with a value L_f, and a three-phase inductor L_g, M_g, common to the two inverters connected in parallel. In this case, the inductance L_{fg} of the general model was not used, so it was considered null.
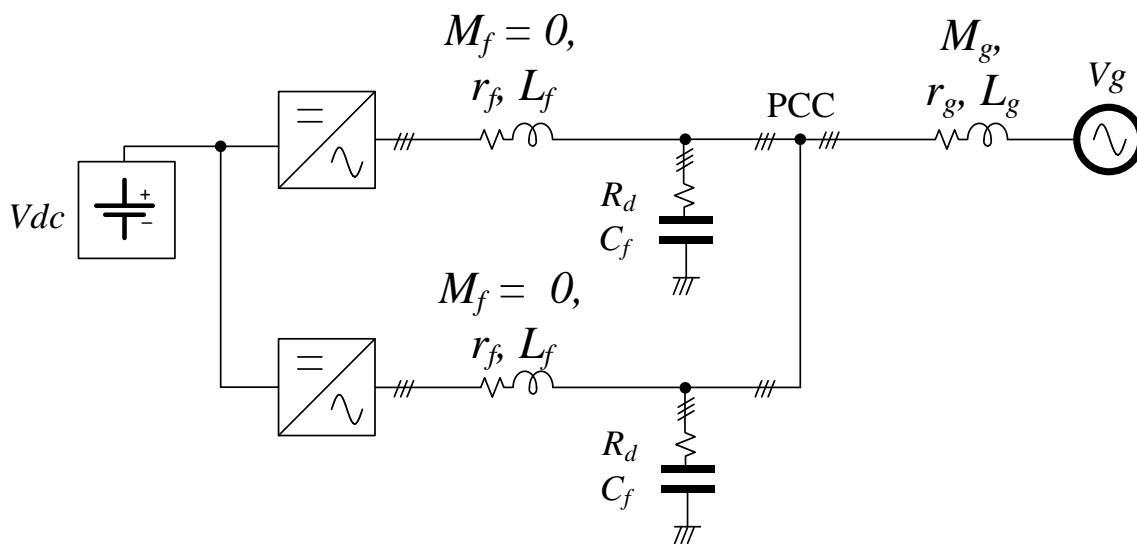

Figure 5. Single-line scheme of two inverters connected in parallel.

Table 4. Parameters of the inverters.

Parameter	Nominal Value	Parameter	Nominal Value
V_g-RMS (phase–phase)	230 V	r_f	50 mΩ
V_{dc}	500 V	r_{fg}	50 mΩ
P_n	5 kW	r_g	50 mΩ
C_o	1.2 mF	C_f	9 μF
L_f	5 mH	R_d	4.4 Ω
L_{fg}	0	f_{sw}	10 kHz
L_g	320 μH	R_s	1 V/A
M_f	0	β	1 V/V
M_{fg}	0	Fm	0.5 V/V
M_g	−80 μH		

The experimental results have been obtained by means of the set-up depicted in Figure 6. Both parallel operating inverters have been connected to the same AC and DC buses and have been controlled using the dual-core Texas Instruments TMS320F28379D microcontroller. The AC bus has been supplied by a bidirectional power supply, Cinergia GL and EL-50, emulating an AC grid of 230 V RMS phase–phase and 50 Hz. Anyway, a GSS Regatron programmable power supply has set the DC bus to 500 V. Table 5 summarizes the test equipment of the experimental set-up.
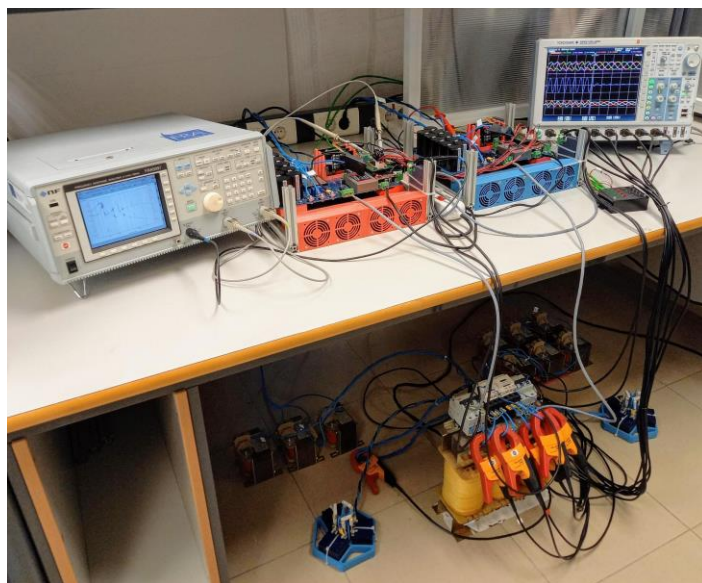
Figure 6. Experimental set-up.

Table 5. Instruments and laboratory material.

AC voltage source	Cinergia GL and EL-50
DC voltage source	GSS Regatron
Current probes	Fluke i400s
Differential voltage probes	Yokogawa 700924
Frequency response analyzer (FRA)	NF Corporation FRA5097
Oscilloscope	Agilent MSO6014A (4 channels, 200 MHz) Yokogawa DLM4038 (8 channels 350 MHz)
Multimeter	Agilent 1241A, Fluke 175, Metrix MX0024
Thermal camera	Fluke Ti25 IR FUSION TECHNOLOGY THERMAL IMAGER

6. Design of the Control Loops

PI controllers are usually used in power converters to implement the regulators of the current control loops in a synchronous reference frame. However, PI controllers have difficulties when the regulated variables have frequency contents close to the crossover frequency of the loops, which is the case of the low-frequency harmonics of the circulating currents. To address this issue, second-order generalized integrators (SOGI) [24] have been added to the *o*-channel controllers to increase their gain at the frequency of the circulating currents' low-frequency harmonics, resulting in PI + SOGI *o*-channel controllers. As it will be seen in the simulation and experimental results section, when the powers provided by the parallel inverters are balanced, the circulating currents present third-order harmonics (150 Hz) and their odd multiples, with the ninth one being the most significant harmonic (450 Hz). Nevertheless, if the power provided by one of the parallel inverters becomes unbalanced, a large fundamental harmonic (50 Hz) appears at the circulating current. Therefore, the SOGIs of the o-channel current controllers are tuned to 50 Hz, 150 Hz, and 450 Hz.

The expressions of the current controllers should be chosen by taking the following issues into account. First, the crossover frequency of the current control loop gains must be higher than the frequency of the harmonics of the variables to be controlled. In addition, the loop gain must be much lower (around 1 decade) than the switching frequency to avoid large signal instabilities and noise problems. In addition, appropriate stability margins must be achieved, typically a phase margin PM > 45° and a gain margin GM > 6 dB. Equations (29) and (34) show the expressions of the chosen current regulators on the *d*- and *q*-axis and on the *o*-axis, respectively. The transfer functions of the *d* and *q* current channels were similar, so that their controllers could agree. The current controllers in both channels were proportional integral regulators. As indicated above, the current regulator in the zero-sequence channel was a PI + SOGIs one, being the generalized integrators tuned at 50 Hz, 150 Hz, and 450 Hz. The bandwidth of the 50 Hz SOGI was 10 Hz, and its gain was 4. The gain of the 150 Hz SOGI was 4, whereas that of the 450 Hz SOGI was 0.5. The bandwidths of the 150 Hz and 450 Hz SOGIs were reduced, with regard to the bandwidth of the 50 Hz SOGI. The reason for that was to avoid the risk of instability, due to a phase loss close to the crossover frequency of the *o*-channel current loops.

$$G_i(s) = PI_i(s) = 0.1 + \frac{10}{s} \tag{29}$$

$$PI_o(s) = 0.2 + \frac{10}{s} \tag{30}$$

$$R_{50}(s) = \frac{4{\cdot}10{\cdot}s}{s^2 + 10s + (2\tau\omega)^2} \tag{31}$$

$$R_{150}(s) = \frac{4{\cdot}\frac{10}{3}s}{s^2 + \frac{10}{3}s + (2\tau3\omega)^2} \tag{32}$$

$$R_{450}(s) = \frac{0.5{\cdot}\frac{10}{9}s}{s^2 + \frac{10}{9}s + (2\tau9\omega)^2} \tag{33}$$

$$G_{io}(s) = PI_o(s) + R_{50}(s) + R_{150}(s) + R_{450}(s) \tag{34}$$

Figure 7a–c depict the Bode plot measurements and the theoretical curves (gain in dB, phase in deg) of the current loop gains: T_{id} ($j\omega$) Equation (26), T_{iq} ($j\omega$) Equation (27), and T_{io} ($j\omega$) Equation (28). The theoretical plots have been obtained by Matlab R2018b. The experimental measurements of Figure 7 have been carried out by means of a frequency response analyzer FRA5097 from NF Corporation. Figure 7d depicts the Bode plot measurements of the current loop gain in the *o*-channel.

As it can be seen from those figures, the current loop frequency response predicted by the developed model was reasonably close to the experimental measurements, so the

developed model was validated as a design and analysis tool. Note that stability was guaranteed in all cases. Specifically, the crossover frequency of the current loops ranged from 680 Hz to 800 Hz, having, in the worst case, the phase margin PM = 47° and the gain margin GM = 7.2 dB.
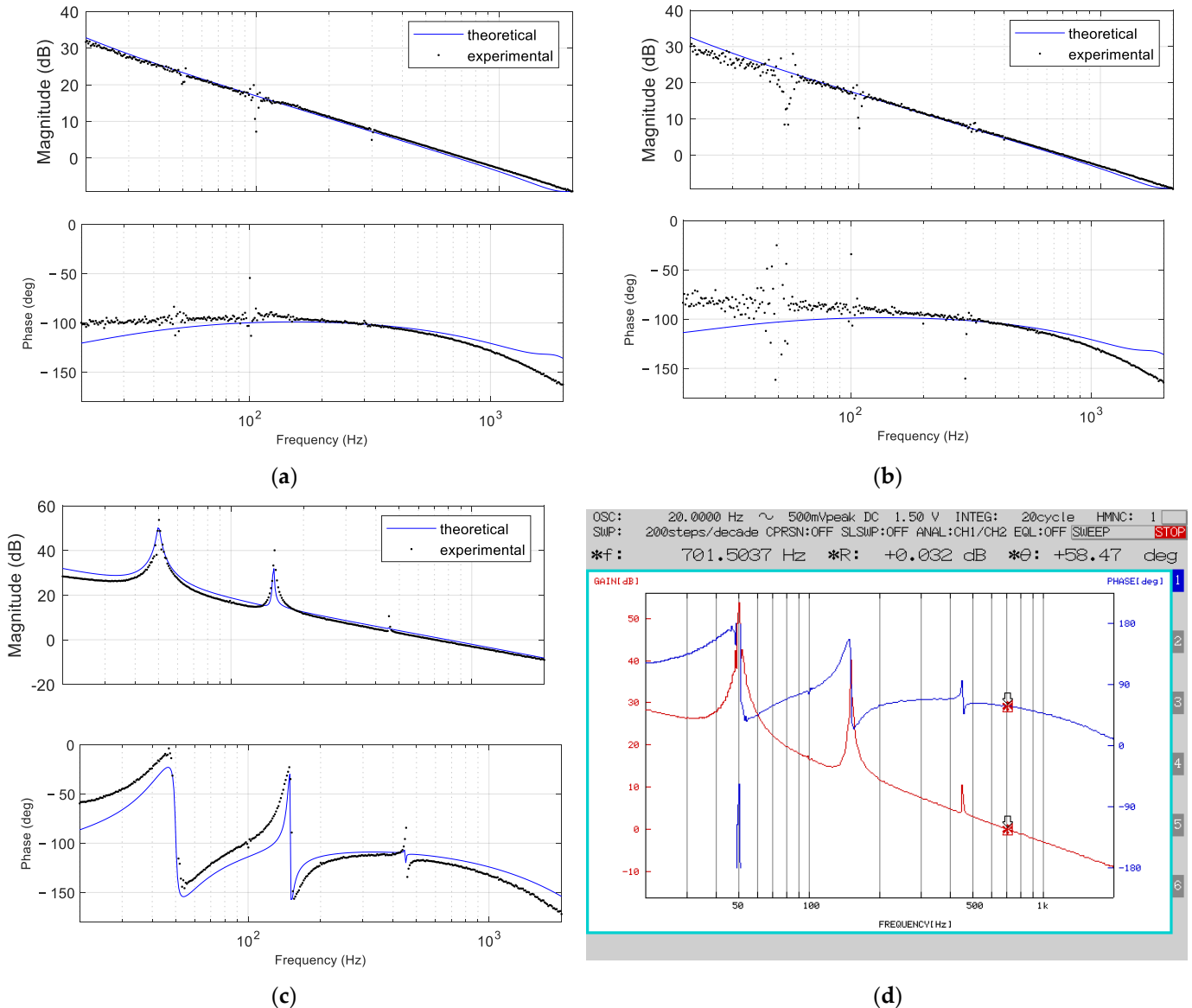

Figure 7. Predicted and measured current control loops gain: (**a**) *d*-axis, (**b**) *q*-axis, and (**c**) *o*-axis. (**d**) Measured current control loop gain in the *o*-axis where *f stands for the crossover frequency, and *R and *θ for the gain and the phase of the control loop at this frequency.

The stability of the system has been also analysed by considering variations of L_f in the range between 5–7 mH. Figure 8a,b represent the pole-zero map in the *d*- and *q*-axis, respectively. It can be seen that, for higher values of L_f, the system is slower and more stable. Figure 8c shows that the L_f variations do not affect the *o*-axis stability. The position of the closed loop pole trajectories has been represented in these figures. It can be seen that, for higher values of K_p, the current control loops become faster, compromising the system stability.
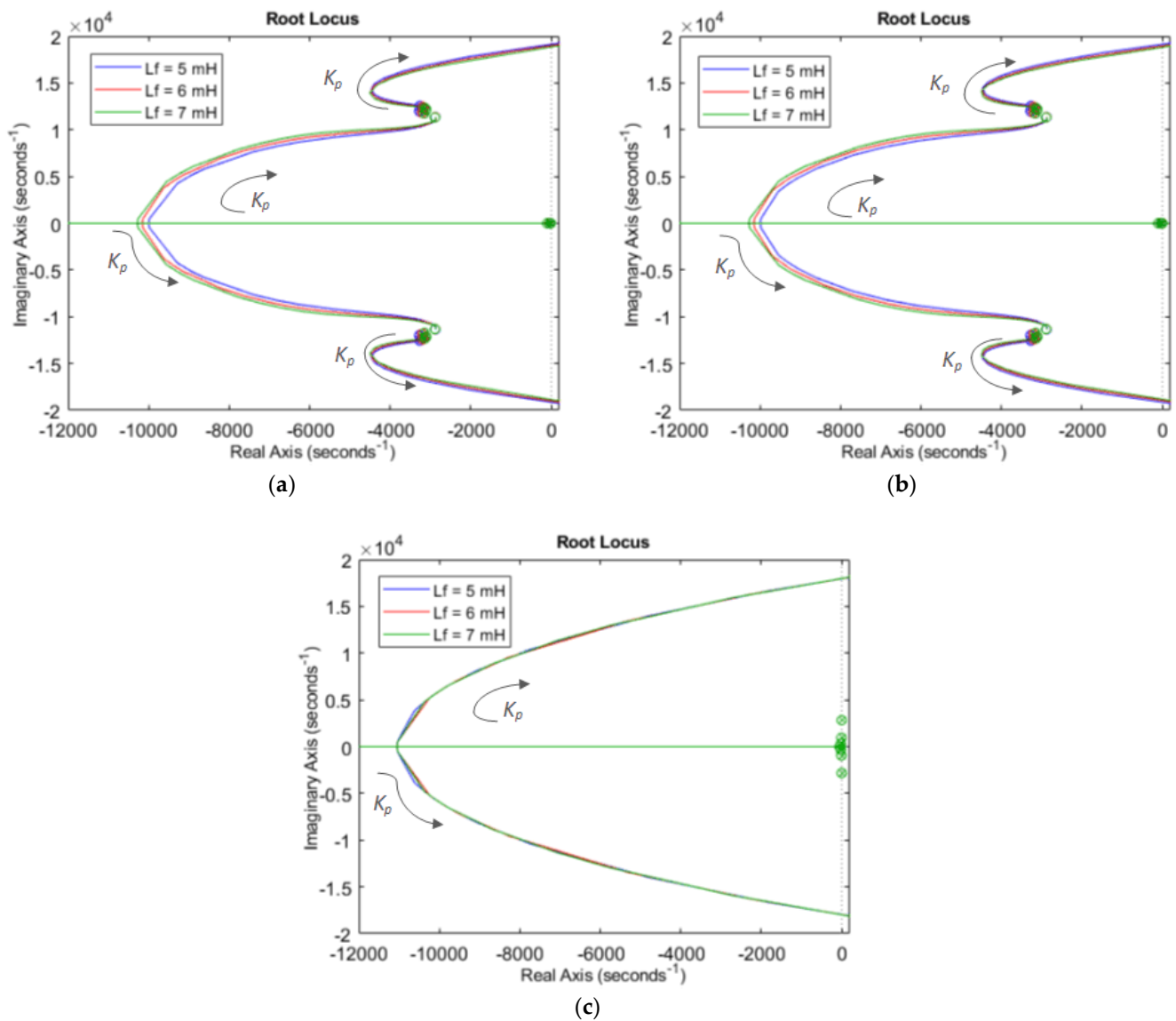
Figure 8. Pole-zero map considering several L_f values: (**a**) *d*-axis, (**b**) *q*-axis and (**c**) *o*-axis.

7. Simulation and Experimental Results

In this section, the simulation and experimental results that validate the proposed control scheme for the suppression of circulating currents are shown. The prototype has been tested by considering that low-frequency circulating currents are due to various reasons: an inductance value mismatch in the phases of the same inverter and among different inverters, power unbalance among inverters, and the use of different PWM modulators in each inverter. In practice, the last scenario happens if the inverter that does not need to regulate the homopolar component (#1 in Figure 3) implements 2D-SVM, instead of 3D-SVM.

Simulation results have been obtained by considering two and three inverters with the characteristics of Table 4 connected in parallel. The experimental results with two inverters connected in parallel have been presented. Only one of the previously described reasons for unbalance has been studied in each experiment.

7.1. Simulation Results

7.1.1. Two Inverters Connected in Parallel

The simulation results, when two 5 kW inverters are connected in parallel, have been obtained by means of PSIM™ 10.0 and are depicted in Figure 9. In this figure, the circulating currents are represented before and after the activation of the zero-sequence control at *t* = 0.25 s. The upper part of each of the graphs corresponds to the phase currents of inverter #1, the lower part depicts the phase currents of inverter #2, and in the central part, the circulating currents are shown.
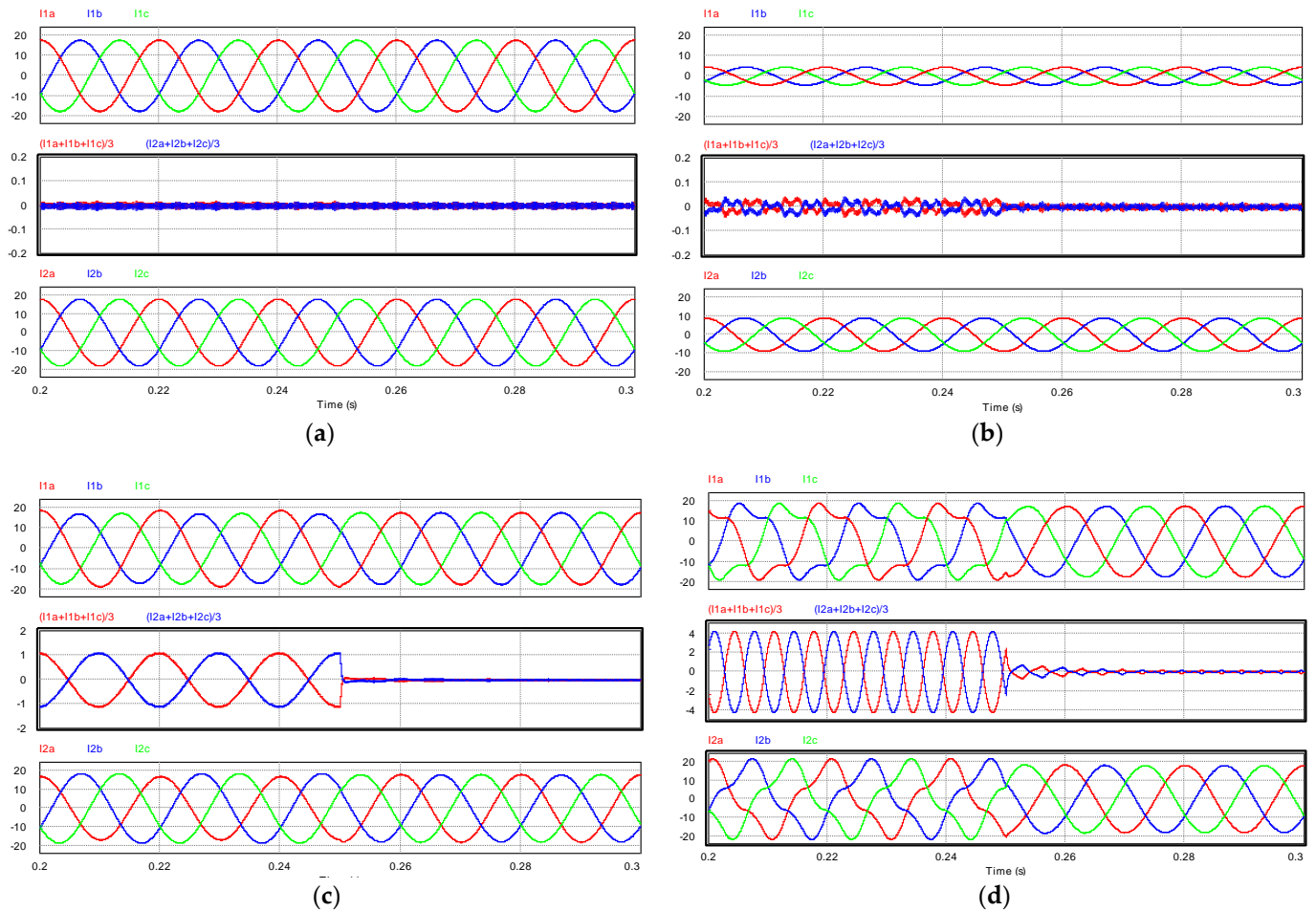

Figure 9. Simulation results of the control of the circulating currents of two inverters connected in parallel (**a**) with unbalanced inductances in both inverters, (**b**) with unbalanced load factor between inverters, (**c**) with unbalanced inductances in the same inverter, (**d**) with a different modulation in each inverter.

Figure 9a shows the simulation results when the value of the inverter side inductances of inverter #2, L_f, is modified to 7 mH. Despite the fact that the circulating currents are inherently small, without the need to control the zero-sequence component, it was found that, with the proposed control of the zero-sequence channel, the 150 Hz component decreased significantly. As described in Section 6, when the currents provided by the inverters are balanced, the circulating current is composed of a three-order harmonic and its odd multiples if there are mismatches in the value of L_f among inverters and in other cases, as will be shown by the experimental results shown in the following.

Figure 9b shows the simulation results when the load factor of the two inverters becomes unbalanced, so that inverter #1 handles 25% of its nominal power, whereas inverter #2 handles 50% of its nominal power. In this case, the circulating currents are of a higher value than in the case in which the inductances of both inverters are unbalanced,

so it is easier to see that the zero-sequence control allows the circulating currents to be significantly reduced.

Figure 9c shows the results when the inductance of phase A of the second inverter is 7 mH, instead of 5 mH. In this case, the circulating current had a large fundamental harmonic, and the phase currents became unbalanced. After activating the zero-sequence control at t = 0.25 s, the circulating current was significantly reduced, leading to a good balancing of the currents, provided by both inverters.

Finally, in Figure 9d, the cases of using a 2D-SVM modulator in inverter #1 and a 3D-SVM modulator in inverter #2 are depicted. In this case, the amplitude of the 150 Hz fundamental component of the circulating current was approximately 4 A, being drastically reduced after activating the zero-sequence component control. It should also be noted that the currents in the phases of each inverter are no longer strongly distorted and are transformed into 50 Hz sinusoidal signals.

7.1.2. Three Inverters Connected in Parallel

In this section, the proposed technique has been applied to three inverters of 5 kW connected in parallel. Since $n - 1$ zero-sequence current control loops are needed to control the circulating currents, the zero-sequence component of the phase currents in inverters #2 and #3 have been controlled.

Figure 10a shows the simulation results with a mismatch in the nominal value of the inductances among inverters. Specifically, L_f in inverter #1 had a value of 5 mH, L_f in inverter #2 had a value of 7 mH, and L_f in inverter #3 was 6 mH. Figure 10b represents the phase currents and the circulating currents when inverter #1, inverter #2, and inverter #3 handled 25%, 30%, and 50% of their nominal power, respectively. Figure 10c depicts the case in which there was a mismatch among the inductances of each phase of the inverter. The phase B inductance of inverter #1 was 6 mH, and the phase A inductance of inverter #2 was 7 mH, instead of 5 mH. Finally, in Figure 10d, the simulation results are shown with a 2D-SVM modulator in inverter #1 and 3D-SVM modulators in inverters #2 and #3.

Note that these results are very similar to the previous case, and that the circulating currents have been drastically reduced with the proposed control structure.
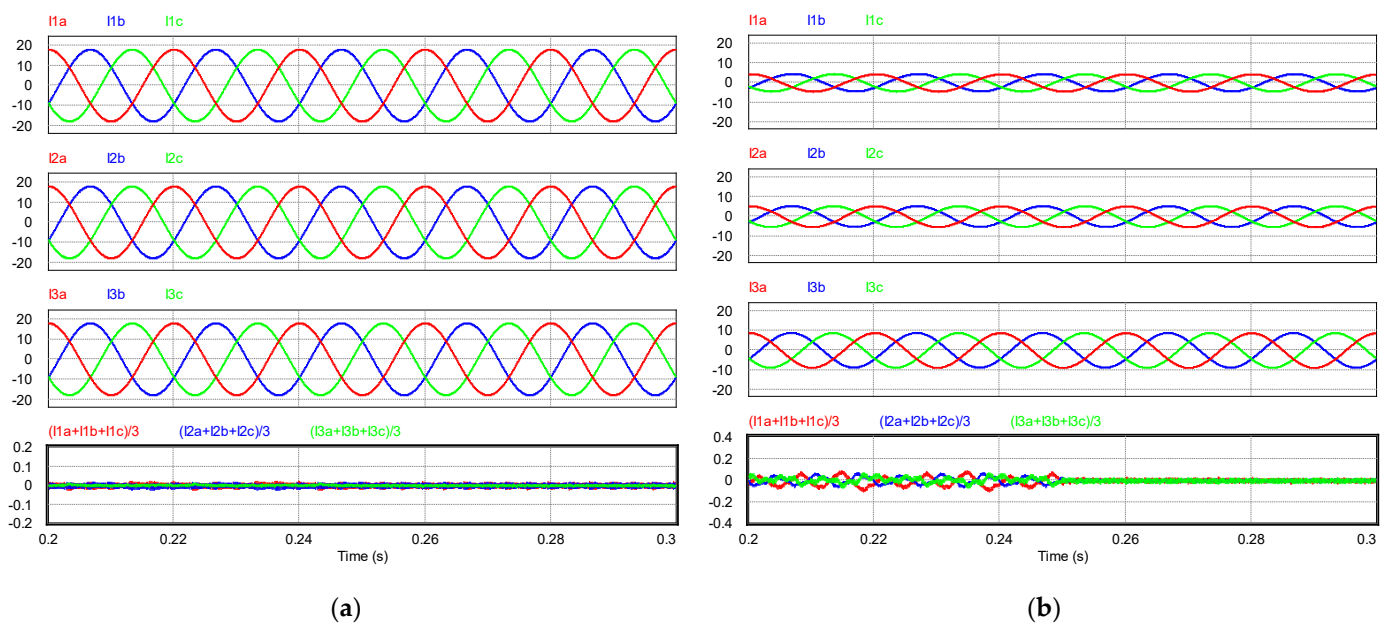

(a)　　　　　　　　　　　　　　　　　　　　　　　**(b)**
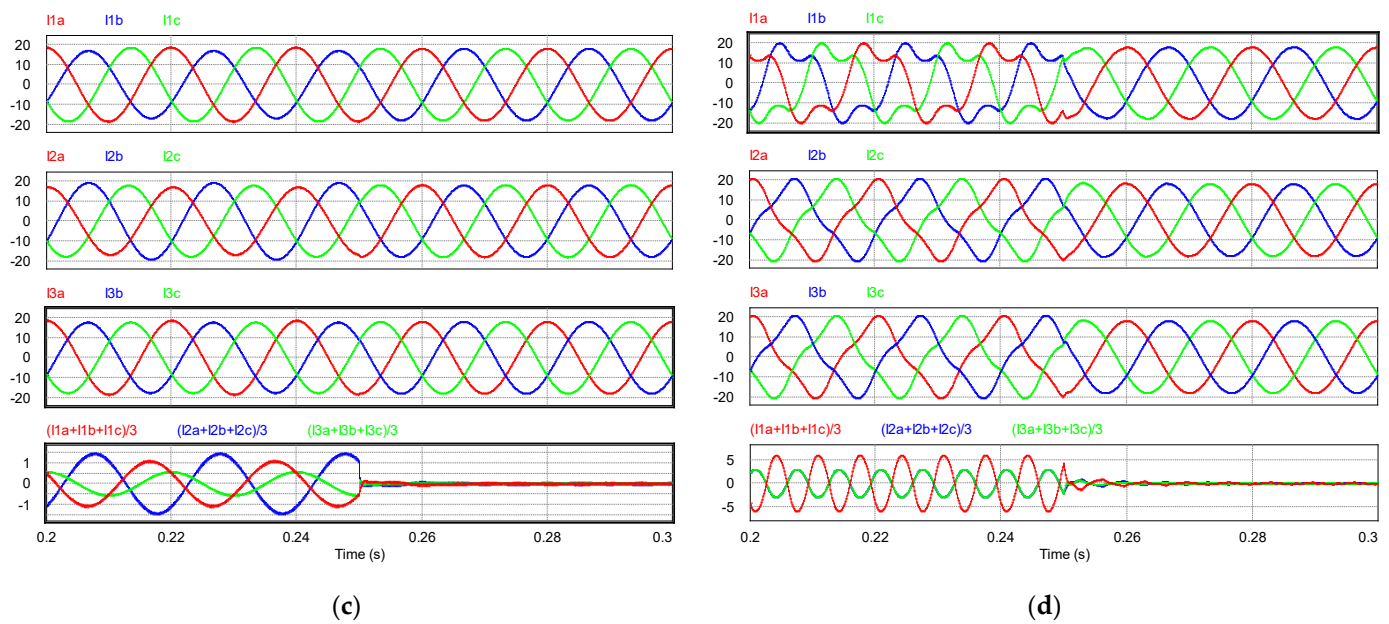
Figure 10. *Cont.*

Figure 10. Simulation results of the control of the circulating currents among three inverters connected in parallel (**a**) with unbalanced inductances in both inverters, (**b**) with unbalanced load factor among inverters, (**c**) with unbalanced inductances in the same inverter, (**d**) with a different modulation in each inverter.

7.2. Experimental Results

In the experimental tests, the factors analyzed in Section 7.1 causing circulating currents have been studied. It should be noted, however, that the experimental results were obtained from real power converters, so it was impossible to study each of the factors in a completely independent way. Indeed, the inductance value used in the grid filter was theoretically 5 mH, but inductances from the same manufacturer have tolerances of up to 20%, even higher in some cases. In this work, inductances with nominal values of 5 mH, 7 mH and tolerances of 10% have been used. To determine the real value of each component, the inductance of each inductor has been measured, resulting in the values collected in Table 6.

At the top of the graphs in Figure 11, the currents in phase A (orange), B (green), and C (pink) of inverter #1 are shown. The phase currents of inverter #2 are shown at the bottom. It should be noted that, in the central part of each graph, the sum of the currents in the phases of inverter #1 ($i_{a1} + i_{b1} + i_{c1}$) are shown in blue, and the sum of the currents of the phases of inverter #2 are represented in pink. These currents are proportional to the circulating currents between inverters, whose expression is $(i_a + i_b + i_c)/3$. A dotted black vertical line marks the activation instant of the proposed control for suppression of the circulating currents.

Figure 11a shows the experimental performance of the proposed control technique, with a mismatch between the inductances of the inverters. In inverter #2, the inductor with a nominal inductance of 5 mH has been replaced by an inductance of 7 mH. The actual values of the inductances used in each phase are summarized in Table 7. The results show that a 50 Hz component appeared in the circulating currents, since the inductance differences among phases did not allow for balancing the phases. A small 150 Hz component also appeared when the grid filter inductances between both inverters were different.

Figure 11b shows the experimental results of the control of circulating currents for a load factor of 25% in inverter #1 and 50% in inverter #2. In this case, the 50 Hz and 150 Hz harmonics also appeared, with the 150 Hz harmonic being greater than in the previous case. The proposed control technique considerably reduced the circulating current.

Figure 11c shows the results in the case in which the inductance connected to phase A of the second inverter was replaced by the inductance L_{f_a2} of 7.16 mH, represented in Table 7. It was observed that, before activating the zero-sequence control, and with both inverters working at their rated power, the sum of the phase currents resulted in a 50 Hz component of about 3.5 A, so the circulating current had a value of about 1.2 A. After activation of the zero-sequence current control, the circulating current was reduced considerably.

Finally, in Figure 11d, inverter #1 works with 2D-SVM and inverter #2 works with 3D-SVM. It was observed that, before activating the control of the zero-sequence component, the currents in the phases were strongly distorted, due to the high value of the 150 Hz component, 4.5 A, that appeared in the circulating current. After the activation of the zero-sequence control, the currents did not exhibit a noticeable distortion.

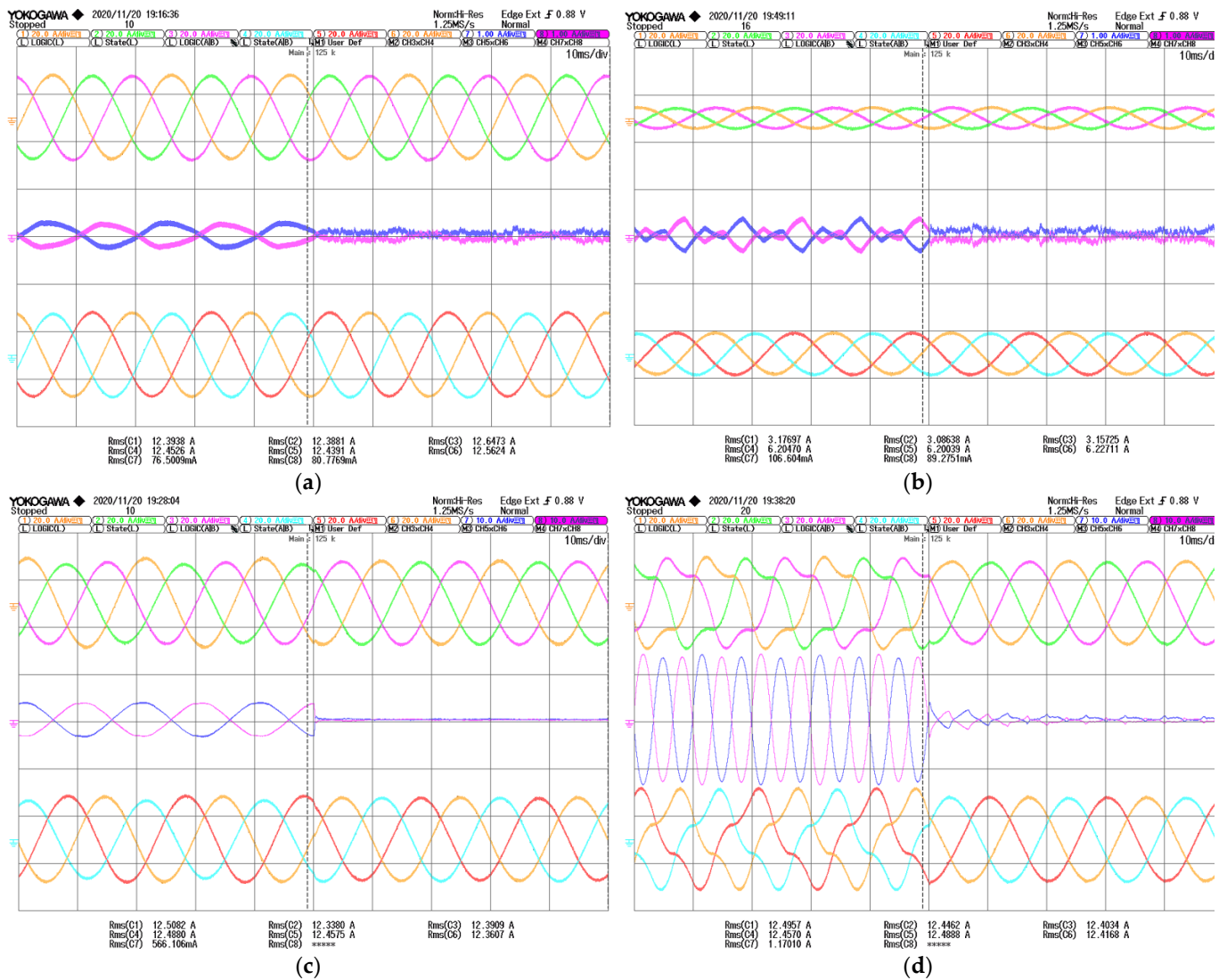**Figure 11.** Experimental results of the control of the circulating currents (**a**) with unbalanced inductances in both inverters, (**b**) with unbalanced load factor between inverters, (**c**) with unbalanced inductances in the same inverter, (**d**) with a different modulation in each inverter. * stands for values that the oscilloscope did not calculate. In this case, the RMS value of Channel 8.

Table 6. Real values of the inductance L_f of 5 mH.

Parameter	Real Value	Parameter	Real Value
L_{f_a1}	5.14 mH	L_{f_a2}	5.1 mH
L_{f_b1}	5.14 mH	L_{f_b2}	4.85 mH
L_{f_c1}	5.27 mH	L_{f_c2}	5.03 mH

Table 7. Real values of the inductance L_f of 7 mH.

Parameter	Real Value
L_{f_a2}	7.16 mH
L_{f_b2}	6.98 mH
L_{f_c2}	7.12 mH

8. Conclusions

This work presents a method for the suppression of low-frequency circulating currents among n three-phase inverters connected in parallel. To this end, a control technique, in which $n - 1$ regulation loops with three-dimensional space vector modulators (3D-SVM), was used to regulate the zero-sequence component of the currents in each inverter. Thus, the circulating currents were controlled as they coincided with the zero-sequence components $(i_o = (i_a + i_b + i_c)/3)$. As a control objective, a zero setpoint value for the zero-sequence has been imposed, so that the circulating currents cancel out.

Several factors that produce circulating currents have been analyzed: mismatches in the inductance values of the grid filters among inverters and in each phase of the same inverter, unbalance of the delivered power, and finally, the use of different modulation techniques. In addition, the harmonic contents of the circulating currents have been considered to adjust resonant controllers in the zero-sequence current loops. This improves the control action at the frequency of the harmonics that form part of the circulating currents.

The simulation and experimental results have been obtained to validate the correct operation of the proposed control. The most relevant cases that can produce circulating currents among inverters connected in parallel have been evaluated in the tests. From the results obtained, we can conclude that the value of the circulating currents in the event of a mismatch among the nominal value of the inductances of each inverter is very low. The same has been observed when the load factor of each inverter was different. However, when there were differences among the phase inductances of the same inverter, the circulating current at nominal power had a high 50 Hz harmonic of 1.2A. With the proposed control technique, this harmonic was reduced to 8 mA (99% attenuation rate). Finally, when inverter #1 was controlled with 2D-SVM and inverter #2 with 3D-SVM, the circulating current had a high 150 Hz harmonic of 4.5 A, which reduced to 100 mA with the zero-sequence current control loop (98% attenuation rate).

Author Contributions: M.L., E.F. and G.G. developed the main idea, the model, and the control of the system; M.L., I.P. and R.G.-M. developed the experimental results; M.L., E.F. and G.G. wrote the paper. All authors have read and agreed to the published version of the manuscript.

Appendix A

In order to obtain the equations in the SRF frame, Equations (8)–(12), (A29 were applied to Equations (3)–(6), where T was the SRF transformation matrix expressed by

Equation (A3). In these equations, ω stands for the grid angular frequency, and x represents any averaged variable (current, voltage, ...).

$$T = \sqrt{\frac{2}{3}} \begin{bmatrix} \cos \omega t & \cos\left(\omega t - \frac{2\pi}{3}\right) & \cos\left(\omega t + \frac{2\pi}{3}\right) \\ -\sin \omega t & -\sin\left(\omega t - \frac{2\pi}{3}\right) & -\sin\left(\omega t + \frac{2\pi}{3}\right) \\ \frac{1}{\sqrt{2}} & \frac{1}{\sqrt{2}} & \frac{1}{\sqrt{2}} \end{bmatrix} \tag{A1}$$

$$\begin{bmatrix} \overline{x}_d \\ \overline{x}_q \\ \overline{x}_o \end{bmatrix} = T \cdot \begin{bmatrix} \overline{x}_a \\ \overline{x}_b \\ \overline{x}_c \end{bmatrix} \leftrightarrow \begin{bmatrix} \overline{x}_a \\ \overline{x}_b \\ \overline{x}_c \end{bmatrix} = T^{-1} \begin{bmatrix} \overline{x}_d \\ \overline{x}_q \\ \overline{x}_o \end{bmatrix} \tag{A2}$$

$$T\frac{dT^{-1}}{dt} = \begin{bmatrix} 0 & -\omega & 0 \\ \omega & 0 & 0 \\ 0 & 0 & 0 \end{bmatrix} \tag{A3}$$

$$T \begin{bmatrix} L_f & M_f & M_f \\ M_f & L_f & M_f \\ M_f & M_f & L_f \end{bmatrix} \frac{dT^{-1}}{dt} \begin{bmatrix} \overline{i}_{1di} \\ \overline{i}_{1qi} \\ \overline{i}_{1oi} \end{bmatrix} = \begin{bmatrix} 0 & -\omega\left(L_f - M_f\right) & 0 \\ \omega\left(L_f - M_f\right) & 0 & 0 \\ 0 & 0 & 0 \end{bmatrix} \begin{bmatrix} \overline{i}_{1di} \\ \overline{i}_{1qi} \\ \overline{i}_{1oi} \end{bmatrix}, \quad i = 1, 2, \dots n \tag{A4}$$

$$T \begin{bmatrix} L_f & M_f & M_f \\ M_f & L_f & M_f \\ M_f & M_f & L_f \end{bmatrix} T^{-1} \begin{bmatrix} \overline{i}_{1di} \\ \overline{i}_{1qi} \\ \overline{i}_{1oi} \end{bmatrix} = \begin{bmatrix} L_f - M_f & 0 & 0 \\ 0 & L_f - M_f & 0 \\ 0 & 0 & L_f + 2M_f \end{bmatrix} \begin{bmatrix} \overline{i}_{1di} \\ \overline{i}_{1qi} \\ \overline{i}_{1oi} \end{bmatrix}, \quad i = 1, 2, \dots n \tag{A5}$$

$$T \begin{bmatrix} L_{fg} + \frac{\sum_{j=1}^{n} c_j}{c_i} L_g & M_{fg} + \frac{\sum_{j=1}^{n} c_j}{c_i} M_g & M_{fg} + \frac{\sum_{j=1}^{n} c_j}{c_i} M_g \\ M_{fg} + \frac{\sum_{j=1}^{n} c_j}{c_i} M_g & L_{fg} + \frac{\sum_{j=1}^{n} c_j}{c_i} L_g & M_{fg} + \frac{\sum_{j=1}^{n} c_j}{c_i} M_g \\ M_{fg} + \frac{\sum_{j=1}^{n} c_j}{c_i} M_g & M_{fg} + \frac{\sum_{j=1}^{n} c_j}{c_i} M_g & L_{fg} + \frac{\sum_{j=1}^{n} c_j}{c_i} L_g \end{bmatrix} \frac{dT^{-1}}{dt} \begin{bmatrix} \overline{i}_{2di} \\ \overline{i}_{2qi} \\ \overline{i}_{2oi} \end{bmatrix}$$
$$= \begin{bmatrix} 0 & -\omega\left(L_{fg} - M_{fg} + \frac{\sum_{j=1}^{n} c_j}{c_i}\left(L_g - M_g\right)\right) & 0 \\ \omega\left(L_{fg} - M_{fg} + \frac{\sum_{j=1}^{n} c_j}{c_i}\left(L_g - M_g\right)\right) & 0 & 0 \\ 0 & 0 & 0 \end{bmatrix} \begin{bmatrix} \overline{i}_{2di} \\ \overline{i}_{2qi} \\ \overline{i}_{2oi} \end{bmatrix}, \tag{A6}$$
$$i = 1, 2, \dots n$$

$$T \begin{bmatrix} L_{fg} + \frac{\sum_{j=1}^{n} c_j}{c_i} L_g & M_{fg} + \frac{\sum_{j=1}^{n} c_j}{c_i} M_g & M_{fg} + \frac{\sum_{j=1}^{n} c_j}{c_i} M_g \\ M_{fg} + \frac{\sum_{j=1}^{n} c_j}{c_i} M_g & L_{fg} + \frac{\sum_{j=1}^{n} c_j}{c_i} L_g & M_{fg} + \frac{\sum_{j=1}^{n} c_j}{c_i} M_g \\ M_{fg} + \frac{\sum_{j=1}^{n} c_j}{c_i} M_g & M_{fg} + \frac{\sum_{j=1}^{n} c_j}{c_i} M_g & L_{fg} + \frac{\sum_{j=1}^{n} c_j}{c_i} L_g \end{bmatrix} T^{-1} \begin{bmatrix} \overline{i}_{2di} \\ \overline{i}_{2qi} \\ \overline{i}_{2oi} \end{bmatrix}$$
$$= \begin{bmatrix} L_{fg} - M_{fg} + \frac{\sum_{j=1}^{n} c_j}{c_i}\left(L_g - M_g\right) & 0 & 0 \\ 0 & L_{fg} - M_{fg} + \frac{\sum_{j=1}^{n} c_j}{c_i}\left(L_g - M_g\right) & 0 \\ 0 & 0 & L_{fg} + 2M_{fg} + \frac{\sum_{j=1}^{n} c_j}{c_i}\left(L_g + 2M_g\right) \end{bmatrix} \begin{bmatrix} \overline{i}_{2di} \\ \overline{i}_{2qi} \\ \overline{i}_{2oi} \end{bmatrix}, \tag{A7}$$
$$i = 1, 2, \dots n$$

$$\left(T^{-1} \begin{bmatrix} \overline{x}_d \\ \overline{x}_q \\ \overline{x}_o \end{bmatrix}\right)^T T^{-1} = \begin{bmatrix} \overline{x}_d \\ \overline{x}_q \\ \overline{x}_o \end{bmatrix}^T \left(T^{-1}\right)^T T^{-1} = \begin{bmatrix} \overline{x}_d \\ \overline{x}_q \\ \overline{x}_o \end{bmatrix}^T \tag{A8}$$

Appendix B

$$A_{\hat{i}12dq\_i12dq} = \begin{bmatrix} \frac{-(R_d+r_f)}{L_f-M_f} & \omega & \frac{R_d}{L_f-M_f} & 0 \\ -\omega & \frac{-(R_d+r_f)}{L_f-M_f} & 0 & \frac{R_d}{L_f-M_f} \\ \frac{R_d}{L_{fg}-M_{fg}+\frac{\sum_{j=1}^{n}c_j}{c_i}(L_g-M_g)} & 0 & \frac{-\left(R_d+r_{fg}+\frac{\sum_{j=1}^{n}c_j}{c_i}r_g\right)}{L_{fg}-M_{fg}+\frac{\sum_{j=1}^{n}c_j}{c_i}(L_g-M_g)} & \omega \\ 0 & \frac{R_d}{L_{fg}-M_{fg}+\frac{\sum_{j=1}^{n}c_j}{c_i}(L_g-M_g)} & -\omega & \frac{-\left(R_d+r_{fg}+\frac{\sum_1^{n}c_i}{c_i}\right)}{L_{fg}-M_{fg}+\frac{\sum_{j=1}^{n}c_j}{c_i}(L_g-M_g)} \end{bmatrix}, \quad (A9)$$

$$i = 1,2,\dots n$$

$$A_{\hat{i}o\_io} = -\frac{r_f+r_{fg}}{L_f+L_{fg}+2M_f+2M_{fg}} \tag{A10}$$

$$A_{\hat{i}12dq\_vcdq} = \begin{bmatrix} -\frac{1}{L_f-M_f} & 0 \\ 0 & -\frac{1}{L_f-M_f} \\ \frac{1}{L_{fg}-M_{fg}+\frac{\sum_{j=1}^{n}c_j}{c_i}(L_g-M_g)} & 0 \\ 0 & \frac{1}{L_{fg}-M_{fg}+\frac{\sum_{j=1}^{n}c_j}{c_i}(L_g-M_g)} \end{bmatrix}, \quad i=1,2,\dots n \tag{A11}$$

$$A_{\hat{i}12dq\_vdc} = \begin{bmatrix} \frac{Fm\cdot D_{di}}{L_f-M_f} \\ \frac{Fm\cdot D_{qi}}{L_f-M_f} \\ 0 \\ 0 \end{bmatrix}, \quad i=1,2,\dots n \tag{A12}$$

$$A_{\hat{i}o\_vdc} = \frac{Fm\cdot D_o i}{n(L_f+L_{fg}+2M_f+2M_{fg})}, \quad i=1,2,\dots n \tag{A13}$$

$$A_{\hat{v}cdq\_i12dq} = \begin{bmatrix} \frac{1}{C_f} & 0 & -\frac{1}{C_f} & 0 \\ 0 & \frac{1}{C_f} & 0 & -\frac{1}{C_f} \end{bmatrix} \tag{A14}$$

$$A_{\hat{v}cdq\_vcdq} = \begin{bmatrix} 0 & \omega \\ -\omega & 0 \end{bmatrix} \tag{A15}$$

$$A_{\hat{v}dc\_i12dq} = \begin{bmatrix} -\frac{Fm\cdot D_{di}}{nC_o} & -\frac{Fm\cdot D_{qi}}{nC_o} & 0 & 0 \end{bmatrix}, \quad i=1,2,\dots n \tag{A16}$$

$$A_{\hat{v}dc\_io} = -\frac{Fm\cdot D_{oi}}{nC_o}, \quad i=1,2,\dots n \tag{A17}$$

$$A_{\hat{v}dc\_vdc} = -\frac{K_{vo}}{nC_o} \tag{A18}$$

$$K_{vo} = -\frac{Idc}{Vdc} \tag{A19}$$

$$B_{\hat{i}12dq\_ddq} = \begin{bmatrix} \frac{Fm\cdot Vdc}{L_f-M_f} & 0 \\ 0 & \frac{Fm\cdot Vdc}{L_f-M_f} \\ 0 & 0 \\ 0 & 0 \end{bmatrix} \tag{A20}$$

$$B_{\hat{i}o\_doi} = \frac{(n-1)Fm\overline{v}_{dc}}{n(L_f+L_{fg}+2M_f+2M_{fg})} \tag{A21}$$

$$B_{\hat{i}o\_do} = \frac{-Fm\,\overline{v}_{dc}}{n(L_f + L_{fg} + 2M_f + 2M_{fg})} \tag{A22}$$

$$B_{\hat{i}12dq\_vgdqo} = \begin{bmatrix} 0 & 0 & 0 \\ 0 & 0 & 0 \\ \frac{-1}{L_{fg}-M_{fg}+\frac{\sum_{j=1}^{n}c_j}{c_i}\left(L_g-M_g\right)} & 0 & 0 \\ 0 & \frac{-1}{L_{fg}-M_{fg}+\frac{\sum_{j=1}^{n}c_j}{c_i}\left(L_g-M_g\right)} & 0 \end{bmatrix}, \ i = 1, 2, \ldots n \tag{A23}$$

$$B_{\hat{v}dc\_ddq} = \begin{bmatrix} -\frac{Fm\cdot I_{di}}{nC_o} & -\frac{Fm\cdot I_{qi}}{nC_o} \end{bmatrix}, \quad i = 1, 2, \ldots n \tag{A24}$$

$$B_{\hat{v}dc\_do} = -\frac{Fm\cdot I_{oi}}{nC_o}, \quad i = 1, 2, \ldots n \tag{A25}$$

References

1. Xueguang, Z.; Li, W.; Xiao, Y.; Wang, G.; Xu, D. Analysis and Suppression of Circulating Current Caused by Carrier Phase Difference in Parallel Voltage Source Inverters With SVPWM. *IEEE Trans. Power Electron.* **2018**, *33*, 11007–11020. [CrossRef]
2. Shen, Z.; Jiang, D.; Chen, J.; Qu, R. Circulating Current Reduction for Paralleled Inverters with Modified Zero-CM PWM Algorithm. *IEEE Trans. Ind. Appl.* **2018**, *54*, 3518–3528. [CrossRef]
3. Wang, X.; Qing, H.; Huang, P.; Zhang, C. Modeling and Stability Analysis of Parallel Inverters in Island Microgrid. *Electronics* **2020**, *9*, 463. [CrossRef]
4. Xiao, H.; Xie, S.; Chen, Y.; Huang, R. An Optimized Transformerless Photovoltaic Grid-Connected Inverter. *IEEE Trans. Ind. Electron.* **2011**, *58*, 1887–1895. [CrossRef]
5. Zhang, M.; Song, B.; Wang, J. Circulating Current Control Strategy Based on Equivalent Feeder for Parallel Inverters in Islanded Microgrid. *IEEE Trans. Power Syst.* **2019**, *34*, 595–605. [CrossRef]
6. Zou, Z.-X.; Hahn, F.; Buticchi, G.; Günter, S.; Liserre, M. Interleaved Operation of Two Neutral-Point-Clamped Inverters With Reduced Circulating Current. *IEEE Trans. Power Electron.* **2018**, *33*, 10122–10134. [CrossRef]
7. Narimani, M.; Moschopoulos, G. Improved Method for Paralleling Reduced Switch VSI Modules: Harmonic Content and Circulating Current. *IEEE Trans. Power Electron.* **2014**, *29*, 3308–3317. [CrossRef]
8. Chen, T.-P. Zero-Sequence Circulating Current Reduction Method for Parallel HEPWM Inverters Between AC Bus and DC Bus. *IEEE Trans. Ind. Electron.* **2012**, *59*, 290–300. [CrossRef]
9. Mazumder, S.K. A Novel Discrete Control Strategy for Independent Stabilization of Parallel Three-Phase Boost Converters by Combining Space-Vector Modulation with Variable-Structure Control. *IEEE Trans. Power Electron.* **2003**, *18*, 1070–1083. [CrossRef]
10. Pan, C.-T.; Liao, Y.-H. Modeling and Control of Circulating Currents for Parallel Three-Phase Boost Rectifiers with Different Load Sharing. *IEEE Trans. Ind. Electron.* **2008**, *55*, 2776–2785. [CrossRef]
11. Ye, Z.; Boroyevich, D.; Lee, F.C. Modeling and Control of Zero-Sequence Current in Parallel Multi-Phase Converters. In Proceedings of the 2000 IEEE 31st Annual Power Electronics Specialists Conference (Cat. No.00CH37018), Galway, Ireland, 23 June 2000; Volume 2, pp. 680–685.
12. Shao, Z.; Zhang, X.; Wang, F.; Cao, R. Modeling and Elimination of Zero-Sequence Circulating Currents in Parallel Three-Level T-Type Grid-Connected Inverters. *IEEE Trans. Power Electron.* **2015**, *30*, 1050–1063. [CrossRef]
13. Zhang, P.; Zhang, G.; Du, H. Circulating Current Suppression of Parallel Photovoltaic Grid-Connected Converters. *IEEE Trans. Circuits Syst. II Express Briefs* **2018**, *65*, 1214–1218. [CrossRef]
14. Ogasawara, S.; Takagaki, J.; Akagi, H.; Nabae, A. A Novel Control Scheme of a Parallel Current-Controlled PWM Inverter. *IEEE Trans. Ind. Appl.* **1992**, *28*, 1023–1030. [CrossRef]
15. Ye, Z.; Boroyevich, D.; Choi, J.-Y.; Lee, F. Control of Circulating Current in Two Parallel Three-Phase Boost Rectifiers. *IEEE Trans. Power Electron.* **2002**, *17*, 609–615. [CrossRef]
16. Chen, T. Dual-Modulator Compensation Technique for Parallel Inverters Using Space-Vector Modulation. *IEEE Trans. Ind. Electron.* **2009**, *56*, 3004–3012. [CrossRef]
17. Prasad, J.S.S.; Ghosh, R.; Narayanan, G. Common-Mode Injection PWM for Parallel Converters. *IEEE Trans. Ind. Electron.* **2015**, *62*, 789–794. [CrossRef]
18. Hou, C. A Multicarrier PWM for Parallel Three-Phase Active Front-End Converters. *IEEE Trans. Power Electron.* **2013**, *28*, 2753–2759. [CrossRef]
19. Liberos, M.; González-Medina, R.; Garcerá, G.; Figueres, E. Modelling and Control of Parallel-Connected Transformerless Inverters for Large Photovoltaic Farms. *Energies* **2017**, *10*, 1242. [CrossRef]

20. Figueres, E.; Garcera, G.; Sandia, J.; Gonzalez-Espin, F.J.; Calvo, J.; Vales, M. Dynamic Analysis of Three-Phase Photovoltaic Inverters with a High Order Grid Filter. In Proceedings of the 2007 IEEE International Symposium on Industrial Electronics, Vigo, Spain, 4–7 June 2007; pp. 691–696.
21. Mohd, A.; Ortjohann, E.; Hamsic, N.; Sinsukthavorn, W.; Lingemann, M.; Schmelter, A.; Morton, D. Control Strategy and Space Vector Modulation for Three-Leg Four-Wire Voltage Source Inverters under Unbalanced Load Conditions. *IET Power Electron.* **2010**, *3*, 323–333. [CrossRef]
22. Albatran, S.; Fu, Y.; Albanna, A.; Schrader, R.; Mazzola, M. Hybrid 2D-3D Space Vector Modulation Voltage Control Algorithm for Three Phase Inverters. *IEEE Trans. Sustain. Energy* **2013**, *4*, 734–744. [CrossRef]
23. Saleh, K.; Sumner, M. A SVM-3D Based Encoderless Control of a Fault-Tolerant PMSM Drive. *Electronics* **2020**, *9*, 1095. [CrossRef]
24. Abdali Nejad, S.; Matas, J.; Elmariachet, J.; Martín, H.; de la Hoz, J. SOGI-FLL Grid Frequency Monitoring with an Error-Based Algorithm for a Better Response in Face of Voltage Sag and Swell Faults. *Electronics* **2021**, *10*, 1414. [CrossRef]